Inorg. Chem. **2008**, *47*, 6056−6071

Structural and Electronic Properties of the [FeFe] Hydrogenase H-Cluster in Different Redox and Protonation States. A DFT Investigation

Maurizio Bruschi,*,† Claudio Greco,‡ Piercarlo Fantucci,‡ and Luca De Gioia*,‡

Department of Environmental Science, University of Milano-Bicocca, Piazza della Scienza 1 20126-Milan (Italy), and Department of Biotechnology and Biosciences, University of Milano-Bicocca, Piazza della Scienza 2 20126-Milan (Italy)

Received April 7, 2008

The molecular and electronic structure of the $\mathbf{Fe_6S_6}$ H-cluster of [FeFe] hydrogenase in relevant redox and protonation states have been investigated by DFT. The calculations have been carried out according to the broken symmetry approach and considering different environmental conditions. The large negative charge of the H-cluster leads, in a vacuum, to structures different from those observed experimentally in the protein. A better agreement with experimental data is observed for solvated complexes, suggesting that the protein environment could buffer the large negative charge of the H-cluster. The comparison of $\mathbf{Fe_6S_6}$ and $\mathbf{Fe_2S_2}$ DFT models shows that the presence of the $\mathbf{Fe_4S_4}$ moiety does not affect appreciably the geometry of the $[2Fe]_H$ cluster. In particular, the $\mathbf{Fe_4S_4}$ cluster alone cannot be invoked to explain the stabilization of the μ-CO forms observed in the enzyme (relative to all-terminal CO species). As for protonation of the hydrogen cluster, it turned out that μ-H species are always more stable than terminal hydride isomers, leading to the conclusion that specific interactions of the H-cluster with the environment, not considered in our calculations, would be necessary to reverse the stability order of μ-H and terminal hydrides. Otherwise, protonation of the metal center and H_2 evolution in the enzyme are predicted to be kinetically controlled processes. Finally, subtle modifications in the H-cluster environment can change the relative stability of key frontier orbitals, triggering electron transfer between the $\mathbf{Fe_4S_4}$ and the Fe_2S_2 moieties forming the H-cluster.

Introduction

Hydrogenases are enzymes that catalyze the reversible reaction $2H^+ + 2e^- \rightarrow H_2$. They bind transition metal ions and, according to their metal content, are classified as [NiFe] or [FeFe] hydrogenases.[1] Also, enzymes previously classified as metal-free hydrogenases have been recently shown to include an iron-containing cofactor.[2]

[FeFe] hydrogenases contain a peculiar $\mathbf{Fe_6S_6}$ cluster, referred to as the H-cluster. X-ray crystallographic studies of the enzyme from *Clostridium pasteurianum* (Cp)[3] and *Desulfovibrio Desulfuricans* (Dd)[4] have revealed that the H-cluster is composed by a classical $\mathbf{Fe_4S_4}$ cluster that is bridged, via the sulfur atom of a cysteine residue, to a biologically unusual binuclear iron cluster, usually referred to as the $[2Fe]_H$ cluster (Figure 1). In the dinuclear cluster, which is thought to be the site of H_2 production, the two iron ions, hereafter referred to as proximal (Fe_p) and distal (Fe_d) relative to the $\mathbf{Fe_4S_4}$ cluster, are bridged by a sulfur-containing chelating ligand that has been proposed to correspond either to 1,3-propanedithiolate (pdt) or di(thiomethyl)amine (dtma).

Several redox states of [FeFe] hydrogenases have been experimentally characterized. The X-ray crystallographic structures solved so far correspond to the H_{ox} form, which is characterized by a CO ligand bridging the two iron atoms of the $[2Fe]_H$ cluster and a free coordination site on the Fe_d atom, and to the H_{red} form, in which the bridging CO moves to a semibridging position.[5] EPR, ENDOR, magnetic circular dichroism, Mössbauer, Resonance Raman, and Fourier-transform infrared spectroscopy studies led to the conclusion

* To whom correspondence should be addressed. E-mail: maurizio.bruschi@unimib.it (M.B.) Fax: +39.02.64483478, E-mail: luca.degioia@unimib.it (L.D.G.), Fax: +39.02.64482890.
† Department of Environmental Science.
‡ Department of Biotechnology and Biosciences.

10.1021/ic8006298 CCC: $40.75
Published on Web 06/10/2008

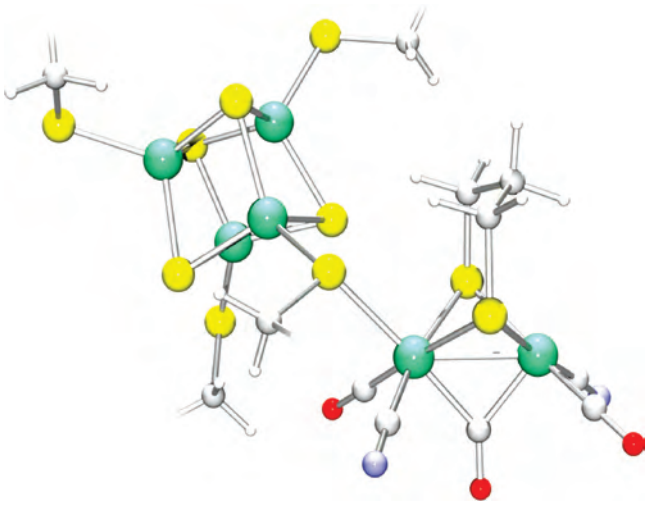

Figure 1. Structure of the H-cluster found in the active site of [FeFe] hydrogenases (atoms are colored as follows: S, yellow; Fe, green; O, red; N, blue).

that in the paramagnetic H_{ox} form the two iron atoms of the $[2Fe]_H$ cluster are in the [Fe(I), Fe(II)] redox state, whereas in the EPR silent H_{red} form both iron atoms should be in the formal [Fe(I), Fe(I)] redox state.[6–8]

[FeFe] hydrogenases are widely studied also for their biotechnological relevance. In fact, H_2 production will become even more important in the near future,[9] and consequently several research groups are presently involved in the design and synthesis of biomimetic compounds related to the $[2Fe]_H$ subcluster.[10] However, it must be noted that all models synthesized so far are drastically less efficient than the enzyme in catalyzing proton reduction and often fail to mimic the precise orientation of the ligands around the bimetallic cluster. These observations may suggest that the environment plays a crucial role in tuning the stereoelectronic properties of the $[2Fe]_H$ cluster. In particular, the proximity of the $\mathbf{Fe_4S_4}$ moiety to the $[2Fe]_H$ cluster suggests that the former could influence the electronic and molecular structure of the binuclear cluster, possibly modulating its catalytic properties. Indeed, a role for the $\mathbf{Fe_4S_4}$ cluster in electron transfer is very likely, despite the fact that it appears to have an extremely low reduction potential.[11]

Even though experimental[1–10] and computational[12–14] studies of enzymes and synthetic models have shed light on crucial aspects of [FeFe] hydrogenase chemistry, the chemical properties of the $\mathbf{Fe_6S_6}$ cluster, and consequently key factors crucial for catalysis, are not fully understood.[11] In fact, the peculiar properties of the isolated H-cluster have remained inaccessible until Pickett and collaborators[15] reported the synthesis and characterization of a model

(1) (a) Albracht, S. P. *Biochim. Biophys. Acta* **1994**, *167*, 1188. (b) Graf, E. G.; Thauer, R. K. *FEBS Lett.* **1981**, *165*, 136. (c) Adams, M. W. W. *Biochim. Biophys. Acta* **1990**, *115*, 1020. (d) Cammack, R. *Nature* **1999**, *214*, 397. (e) Nicolet, Y.; Lemon, B. J.; Fontecilla-Camps, J. C.; Peters, J. W. *Trends Biochem. Sci.* **2000**, *138*, 25. (f) Peters, J. W. *Curr. Opin. Struct. Biol.* **1999**, *670*, 9. (g) Horner, D. S.; Heil, B.; Happe, T.; Embley, T. M. *Trends Biochem. Sci.* **2002**, *148*, 27. (h) Nicolet, Y.; Cavazza, C.; Fontecilla-Camps, J. C. J. *Inorg. Biochem.* **2002**, *1*, 91. (i) *Hydrogen as Fuel - Learning from Nature*; Cammack, R., Frey, M., Robson, R., Eds; London: Taylor and Francis, 2001. (j) Vincent, K. A.; Cracknell, J. A.; Parkin, A.; Armstrong, F. A. *Dalton Trans.* **2005**, 3397.

(2) (a) Lyon, E. J.; Shima, S.; Buurman, G.; Chowdhuri, S.; Batschauer, A.; Steinbach, K.; Thauer, R. K. *Eur. J. Biochem.* **2004**, *271*, 195. (b) Pilak, O.; Mamat, B.; Vogt, S.; Hagemeier, C. H.; Thauer, R. K.; Shima, S.; Vonrhein, C.; Warkentin, E.; Ermler, U. *J. Mol. Biol.* **2006**, *358*, 798. (c) Korbas, M.; Vogt, S.; Meyer-Klaucke, W.; Bill, E.; Lyon, E. G.; Thauer, R., K.; Shima, S. *J. Biol. Chem.* **2006**, *281*, 30804.

(3) Peters, J. W.; Lanzilotta, W. N.; Lemon, B. J.; Seefeldt, L. C. *Science* **1998**, *282*, 1853.

(4) Nicolet, Y.; Piras, C.; Legrand, P.; Hatchikian, E. C.; Fontecilla-Camps, J. C. *Structure* **1999**, 7.

(5) Nicolet, Y.; de Lacey, A. L.; Vernède, X.; Fernandez, V. M.; Hatchikian, E. C.; Fontecilla-Camps, J. C. *J. Am. Chem. Soc.* **2001**, *123*, 1596.

(6) (a) Hatchikian, E. C.; Forget, N.; Fernandez, V. M.; Williams, R.; Cammack, R. *Eur. J. Biochem.* **1992**, *209*, 357. (b) Pierik, A. J.; Hulstein, M.; Hagen, W. R.; Albracht, S. P. J. *Eur. J. Biochem.* **1998**, *258*, 572. (c) Bennet, B.; Lemon, B. J.; Peters, J. W. *Biochemistry* **2000**, *39*, 7455. (d) Chen, Z. J.; Lemon, B. J.; Huang, S.; Swartz, D. J.; Peters, J. W.; Bangley, K. A. *Biochemistry* **2002**, *41*, 2036. (e) De Lacey, A.; Stadler, C.; Cavazza, C.; Hatchikian, E. C.; Fernandez, V. M. *J. Am. Chem. Soc.* **2000**, *122*, 11232.

(7) (a) Popescu, C. P.; Münck, E. *J. Am. Chem. Soc.* **1999**, *121*, 7877. (b) Pereira, A. S.; Tavares, P.; Moura, I.; Moura, J. J. G.; Huynh, B. H. *J. Am. Chem. Soc.* **2001**, *123*, 2771. (c) Albracht, S. P. J.; Roseboom, W.; Hatchikian, E. C. *J. Biol. Inorg. Chem.* **2006**, *11*, 88.

(8) Lubitz, W.; Reijerse, E.; van Gastel, M. *Chem. Rev.* **2007**, *107*, 4331.

(9) Happe, T.; Hemschemeier, A.; Winkler, M.; Kaminski, A. *Trends Plant. Sci.* **2002**, *7*, 246.

(10) (a) Lyon, E. J.; Georgakaki, I. P.; Reibenspies, J. H.; Darensbourg, M. Y. *Angew. Chem., Int. Ed.* **1999**, *38*, 3178. (b) Le Cloirec, A.; Best, S. P.; Borg, S.; Davies, S. C.; Evans, D. J.; Hughes, D. L.; Pickett, C. J. *Chem. Commun.* **1999**, 2285. (c) Schmidt, M.; Contakes, S. M.; Rauchfuss, T. B. *J. Am. Chem. Soc.* **1999**, *121*, 9736. (d) Georgakaki, I. P.; Miller, M. L.; Darensbourg, M. Y. *Inorg. Chem.* **2003**, *42*, 2489. (e) Zhao, X.; Georgakaki, I. P.; Miller, M. L.; Yarbrouch, J. C.; Darensbourg, M. Y. *J. Am. Chem. Soc.* **2001**, *123*, 9710. (f) Boyke, C. A.; Rauchfuss, T. B.; Ott, S.; Kritikos, M.; Akermark, B.; Sun, L. *Angew. Chem., Int. Ed.* **2003**, *42*, 3285. (g) Wilson, S. R.; Rohmer, M.-M.; Benard, M. *J. Am. Chem. Soc.* **2004**, *126*, 15151. (h) Rauchfuss, T. B. *Inorg. Chem.* **2004**, *43*, 14. (i) Liu, T.; Wang, M.; Shi, Z.; Cui, H.; Dong, W.; Chen, J.; Akermark, B.; Sun, L. *Chem.—Eur. J.* **2004**, *10*, 4474. (j) Evans, D. J.; Pickett, C. *J. Chem. Soc. Rev.* **2003**, *32*, 268. (k) Razavet, M.; Davies, S. C.; Hughes, D. L.; Barclay, J. E.; Evans, D. J.; Fairhurst, S. A.; Liu, X.; Pickett, C. J. *J. Chem. Soc., Dalton Trans.* **2003**, 586. (l) Borg, S. J.; Behrsing, T.; Best, S. P.; Razavet, M.; Liu, X.; Pickett, C. J. *J. Am. Chem. Soc.* **2004**, *126*, 16988. (m) Song, L.-C.; Yang, Z.-Y.; Bian, H.-Z.; Hu, Q.-M. *Organometallics* **2004**, *23*, 3082. (n) Lee, C.-M.; Chen, C.-H.; Ke, S.-C.; Lee, G. H.; Liaw, W.-F. *J. Am. Chem. Soc.* **2004**, *126*, 8406. (o) Tye, J. W.; Lee, J.; Wang, H.-W.; Mejia-Rodriguez, R.; Reibenspies, J. H.; Hall, M. B.; Darensbourg, M. Y. *Inorg. Chem.* **2005**, *44*, 5550. (p) Boyke, C. A.; van der Vlugt, J. I.; Rauchfuss, T. B.; Wilson, S. R.; Zampella, G.; De Gioia, L. *J. Am. Chem. Soc.* **2005**, *127*, 11010. (q) Schwartz, L.; Eilers, G.; Eriksson, L.; Gogoll, A.; Lomoth, R.; Ott, S. *Chem. Commun.* **2006**, 520. (r) Dong, W.; Wang, M.; Liu, X.; Jin, K.; Li, G.; Wang, F.; Sun, L. *Chem. Commun* **2006**, 305. (s) van der Vlugt, J. I.; Rauchfuss, T. B.; Wilson, S. R. *Chem.—Eur. J.* **2006**, *12*, 90. (t) Liu, T.; Daresbourg, M. Y. *J. Am. Chem. Soc.* **2007**, *129*, 7008. (u) Justice, A. K.; Rauchfuss, T. B., Wilson, S. R. *Angew. Chem., Int. Ed.* 2007, ASAP.

(11) Armstrong, F. A. *Curr. Opin. Chem. Biol.* **2004**, *8*, 133.

(12) (a) Cao, Z.; Hall, M. B. *J. Am. Chem. Soc.* **2001**, *123*, 3734. (b) Fan, H.-J.; Hall, M. B. *J. Am. Chem. Soc.* **2001**, *123*, 3828. (c) Liu, Z.-P.; Hu, P. *J. Am. Chem. Soc.* **2002**, *124*, 5175. (d) Bruschi, M.; Fantucci, P.; De Gioia, L. *Inorg. Chem.* **2002**, *41*, 1421. (e) Bruschi, M.; Fantucci, P.; De Gioia, L. *Inorg. Chem.* **2003**, *42*, 4773. (f) Zhou, T.; Mo, Y.; Liu, A.; Zhou, Z.; Tsai, K. R. *Inorg. Chem.* **2004**, *43*, 923. (g) Zhou, T.; Mo, Y.; Zhou, Z.; Tsai, K. *Inorg. Chem.* **2005**, *44*, 4941. (h) Zilberman, S.; Stiefel, E. I.; Cohen, M. H.; Car, R. *J. Phys. Chem. B* **2006**, *110*, 7049. (i) Zilberman, S.; Stiefel, E. I.; Cohen, M. H.; Car, R. *Inorg. Chem.* **2006**, *45*, 5715. (j) Zampella, G.; Greco, C.; Fantucci, P.; De Gioia, L. *Inorg. Chem.* **2006**, *45*, 4109.

(13) Bruschi, M.; Fantucci, P.; De Gioia, L. *Inorg. Chem.* **2004**, *43*, 3733.

(14) Tye, J. W.; Darensbourg, M. Y.; Hall, M. B. *Inorg. Chem.* **2006**, *45*, 1552.

(15) Tard, C.; Liu, X.; Ibrahim, S. K.; Bruschi, M.; De Gioia, L.; Davies, S. C.; Yang, X.; Wang, L.-S.; Sawers, G.; Pickett, C. J. *Nature* **2005**, *433*, 610.

complex closely resembling the enzymatic $\mathbf{Fe_6S_6}$ cluster. Recently, Brunold et al.[16] and Schwab et al.[17] reported the first computational studies in which some of the effects due to the presence of the $\mathbf{Fe_4S_4}$ moiety in the H-cluster have been explored. Moreover, a recent hybrid quantum mechanical/molecular mechanical (QM/MM) study[18] has provided some insights into the effects exerted by the protein environment on H-cluster activation.

With the aim of contributing to the characterization of the peculiar stereoelectronic features of the H-cluster and to better understanding the interplay between the di-iron and cubane units, we have used DFT to study the model complexes $[(CH_3S)_4(Fe_4S_4)(\mu\text{-pdt})(Fe_2)(CO)_3(CN)_2]^{3-/5-}$, as well as their adducts with H^+ and H_2. In particular, both isomers characterized by all-terminal CO ligands (from hereafter labeled with the suffix t) and featuring a μ-CO ligand (from hereafter labeled with the suffix b) have been taken into account for each redox state. To explore the effects of the environment on the electronic and molecular properties of the H-cluster models, geometry optimizations and electronic structure calculations have been carried out in a vacuum ($\epsilon = 1$), and also considering models soaked in a polarizable continuum medium characterized by dielectric constant $\epsilon = 4$ and 40, which are values commonly used to describe a protein environment[19] (from hereafter a subscript will be used as a label to indicate the ϵ value). To better evaluate the influence of the $\mathbf{Fe_4S_4}$ moiety on the binuclear cluster, structural and electronic properties of the whole H-cluster have been compared to those computed, at the same level of theory, for models of the $[2Fe]_H$ cluster.

Computational Details

Geometry optimizations have been carried out using the *Turbomole* suite of programs.[20] The electronic wave function has been determined within the DFT approach, using the BP86 functional[21] and an all-electron valence triple-ζ basis set with polarization functions on all atoms (TZVP).[22] Atomic coordinates of the starting structures were obtained from the X-ray geometry of the H-cluster from the *Clostridium pasteurianum* [FeFe] hydrogenase.[3] Differently from other works,[16,17] geometry optimizations have been performed without imposing any constraints on atoms. The protein environment has been modeled by soaking the H-cluster in a polarizable continuum medium.

The theoretical investigation on the H-cluster is a nontrivial task because the $\mathbf{Fe_4S_4}$ subunit is composed by two $\mathbf{Fe_2S_2}$ layers with high-spin (HS) iron atoms coupled antiferromagnetically to give an overall low-spin ground state. The ground-state wave function of such spin-coupled systems corresponds to a linear combinations of determinants that should require a multiconfigurational treatment, not possible within the DFT scheme. However, in the single determinant approximation, the antiferromagnetic interactions can be modeled according to the broken symmetry (BS) approach, introduced by Noodleman.[23,24] The BS wave function, being of spin-unrestricted type, does not represent a pure-spin state, but a weighted average of pure-spin states (and energies). Further, the spin interaction within the system can be modeled by the Heisenberg Hamiltonian $\hat{\mathbf{H}} = \sum_{i>j} J_{ij}(\hat{\mathbf{S}}_i \cdot \hat{\mathbf{S}}_j)$, in which the summation is extended over all of the couples of spin centers i and j bearing spin S_i and S_j, and J_{ij} is the associated exchange coupling constant. Noodleman showed that the expectation values of each product of spin operators $\hat{S}_i \cdot \hat{S}_j$ for the HS and BS states can be obtained from spin algebra according to:

$$\langle \hat{\mathbf{S}}_i \cdot \hat{\mathbf{S}}_j \rangle_{HS} = +S_i S_j \quad (1)$$

$$\langle \hat{\mathbf{S}}_i \cdot \hat{\mathbf{S}}_j \rangle_{BS} = -S_i S_j \quad (2)$$

Several BS states can be calculated for multiple spin systems by coupling spins at the different centers in a ferromagnetic or antiferromagnetic mode. The J_{ij} parameters can then be determined from the unique HS state and a suitable number of BS states, by means of eqs 1 and 2.

In the oxidized $\mathbf{[Fe_4S_4]^{2+}}$ cluster, the two $\mathbf{Fe_2S_2}$ layers (labeled as **A** and **B** in Figure 2) are coupled antiferromagnetically and generally treated as single-spin centers, composed by Fe^{2+} and Fe^{3+} high-spin ions, with $S = S_1(2) + S_2(^5/_2) = {}^9/_2$. The oxidized form of the H-cluster (H_{ox}), in which an unpaired electron is also localized on the $[2Fe]_H$ cluster (vide infra), can be represented by a three-spin system Hamiltonian of the form:

$$\hat{\boldsymbol{H}} = J_{cube}(\hat{\mathbf{S}}_\mathbf{A} \cdot \hat{\mathbf{S}}_\mathbf{B}) + J_H(\hat{\mathbf{S}}_\mathbf{A} \cdot \hat{\mathbf{S}}_\mathbf{H}) \quad (3)$$

provided that interactions between nonadjacent sites are neglected. In eq 3, J_{cube} represents the exchange interaction constant between the two $\mathbf{Fe_2S_2}$ layers of the diamagnetic $\mathbf{Fe_4S_4}$ cluster with $S_A = S_B = {}^9/_2$, and J_H is the exchange coupling between the vicinal $\mathbf{Fe_2S_2}$ layer (**A**) and the $[2Fe]_H$ cluster with $S_H = {}^1/_2$ (Figure 1). To evaluate J_{cube} and J_H, two BS solutions have been calculated; one in which the coupling of the $\mathbf{Fe_2S_2}$ layer **A** with the $[2Fe]_H$ unit is ferromagnetic (BS_1) and the other one in which this coupling is antiferromagnetic (BS_2). J_{cube} and J_H can then be obtained from energy differences of HS, BS_1, and BS_2 states, using the Hamiltonian (3) and the spin algebra of eqs (1) and (2).

The monoelectron reduction of H_{ox} leads to the EPR silent H_{red} form, where the antiferromagnetic coupling of spins are actually extended only to the two Fe_2S_2 layers of the $\mathbf{[Fe_4S_4]^{2+}}$ cluster (vide infra). The Hamiltonian (3) is then simplified to $\hat{\boldsymbol{H}} = J_{cube}\,\hat{\mathbf{S}}_\mathbf{A} \cdot \hat{\mathbf{S}}_\mathbf{B}$), where $S_A = S_B = {}^9/_2$ and J_{cube} can be calculated from the energy difference of the HS and BS_1 states using the spin algebra of eqs 1 and 2.

A further monoelectron reduction provides the H_{sred} form of the H-cluster in which the Fe_4S_4 cluster is reduced to the $\mathbf{[Fe_4S_4]^{3+}}$ redox state (vide infra). In this case, the two layers of the Fe_4S_4 cluster are constituted by a mixed-valence pair of Fe^{2+} and Fe^{3+} ions ($S = S_1(2) + S_2(^5/_2) = {}^9/_2$), and an all-ferrous pair of Fe^{2+} ions ($S = S_1(2) + S_2(2) = 4$). For such a system, an additional complication occurs because the added electron is localized on the Fe(II)Fe(II) layer in the BS wave function, but it is delocalized over the entire Fe_4S_4 cluster in the HS state. This spin resonance

(16) Flieder, A. T.; Brunold, T. C. *Inorg. Chem.* **2005**, *44*, 9322.
(17) Schwab, D. E.; Tard, C.; Brecht, E.; Peters, J. W.; Pickett, C. J.; Szilagyi, R. K. *Chem. Commun.* **2006**, *35*, 3696.
(18) (a) Greco, C.; Bruschi, M.; De Gioia, L.; Ryde, U. *Inorg. Chem.* **2007**, *46*, 5911–5921. (b) Greco, C.; Bruschi, M.; Heimdal, J.; Fantucci, P.; De Gioia, L.; Ryde, U. *Inorg. Chem.* **2007**, *46*, 7256.
(19) (a) Himo, F.; Noodleman, L.; Blomberg, M. R. A.; Siegbahn, P. E. M. *J. Phys. Chem. A* **2002**, *106*, 8757. (b) Klamnt, A. *J. Phys. Chem.* **1995**, *99*, 2224. (c) Klamnt, A. *J. Phys. Chem.* **1996**, *100*, 3349. (d) Warshel, A.; Naray-Szabo, G.; Sussman, F.; Hwang, J.-K. *Biochemistry* **1989**, *28*, 3629. (e) Bottoni, A.; Lanza, C. Z.; Miscione, G. P.; Spinelli, D. *J. Am. Chem. Soc.* **2004**, *126*, 1542–1550.
(20) Ahlrichs, R.; Bar, M.; Haser, M.; Horn, H.; Kolmel, C. *Chem. Phys. Lett.* **1989**, *162*, 165.
(21) Eichkorn, K.; Weigend, F.; Treutler, O.; Ahlrichs, R. *Theor. Chem. Acc.* **1997**, *97*, 119.
(22) Schafer, A.; Huber, C.; Ahlrichs, R. *J. Chem. Phys.* **1994**, *100*, 5829.
(23) Noodleman, L.; Norman, J. G., Jr *J. Chem. Phys.* **1979**, *70*, 4903.
(24) Noodleman, L. *J. Chem. Phys.* **1981**, *74*, 5737.

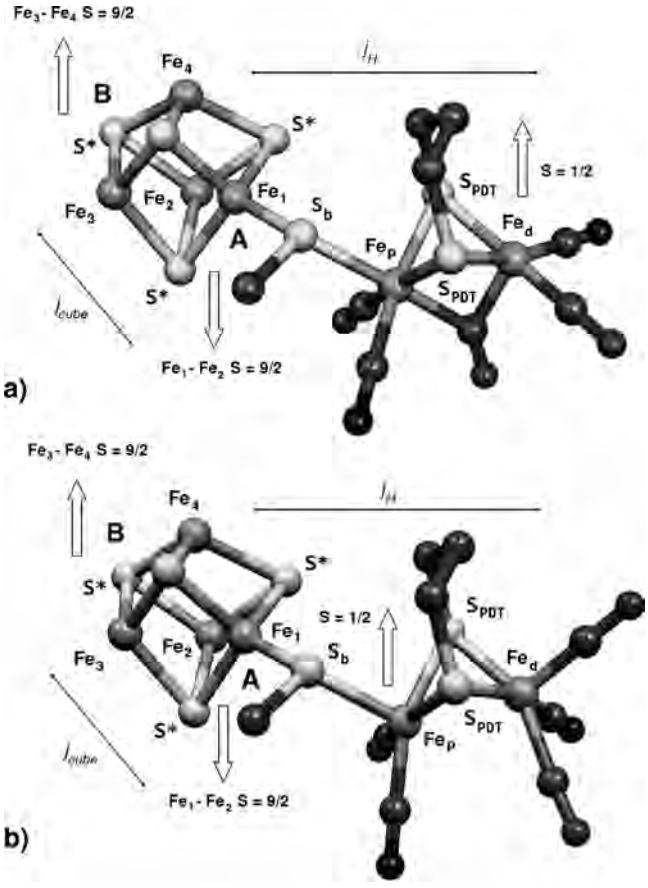

Figure 2. Schematic diagram of the three-spin model for (a) the μ-CO and (b) all-terminal CO forms of the H-cluster. In the reduced state, the Fe_4S_4 cluster is formed by two layers of $\mathbf{Fe_2S_2}$ units indicated in the figure as **A** and **B**. In each unit, the two iron atoms are coupled ferromagnetically, whereas the two units are coupled antiferromagnetically to give the resulting low-spin state. The exchange coupling constants between the two layers, considered as single spin centers is J_{cube}. The $[2Fe]_H$ cluster in the formal [Fe(I), Fe(II)] has one unpaired electron that can be coupled ferromagnetically or antiferromagnetically to the adjacent **A** layer of the cubane. The exchange coupling constants between the $[2Fe]_H$ cluster and the **A** layer is J_H. As indicated in the figure, the unpaired electron in the $[2Fe]_H$ moiety is localized on the Fe_d and Fe_p atoms for the bridged and open forms, respectively.

delocalization reduces the degeneracy of the spin states and can be represented by introducing the term $B'(S + {}^1/_2)$ in the spin Hamiltonian, which therefore is written as,

$$\hat{\boldsymbol{H}} = J_{cube}(\hat{\mathbf{S}}_{\mathbf{A}} \cdot \hat{\mathbf{S}}_{\mathbf{B}}) + B'\left(S + \frac{1}{2}\right) \tag{4}$$

where B' is a resonance delocalization parameter, and S is the total spin quantum number. For the $[Fe_4S_4(SCH_3)_4]^{-3}$ cluster in D_2d symmetry, the B' parameter is calculated within the HS state ($S = {}^{17}/_2$) from the energy splitting of a_2 and b_1 orbitals in D_2d, generated from the a_2 orbital in C_2v.[30] The B' parameter can be used to calculate an average state energy $E(S)_{av(B')}$ by adding the $B'(S_{max} + {}^1/_2)$ term to the energy of the HS state. J_{cube} is computed using the Hamiltonian (4) from the difference between the average state energy of the HS state ($E(HS)_{av(B')}$) and the energy of the BS_1 state.

As noted by Brunold,[16] the iron atoms in the Fe_4S_4 cluster are not equivalent, and therefore up to three different ways of localizing spins could be considered, each of them being characterized by a different definition of the Fe_2S_2 layers. For each of the three schemes of spin localization, BS_1 and BS_2 solutions have been calculated. Therefore, for each relevant species investigated, we computed a total of six BS solutions. In particular (Figure 2 for atom labeling), the three coupling schemes are based on the following sites definition: (i) Fe_1-Fe_2 and Fe_3-Fe_4, (ii) Fe_1-Fe_3 and Fe_2-Fe_4, and (iii) Fe_1-Fe_4 and Fe_2-Fe_3. The schemes (i), (ii), and (iii) are coupled with $[2Fe]_H$ according to BS_1 and BS_2. All values reported for these species correspond to the arithmetic mean of these six possible BS configurations. For each value, the standard deviation is also reported.

The BS wave functions have been obtained starting from single-point energy calculations of the distinct $[Fe_iFe_jS_2(SCH_3)_2]$, $[Fe_kFe_lS_2(SCH_3)_2]$, and $[Fe_pFe_d(CO)_3(CN)_2(PDT)]$ molecular fragments in their fixed initial geometries. Converged spin-α and spin-β molecular orbitals have been used as initial guess for the BS calculation. Spin population has been determined by the Mulliken analysis. Effects due to the environment have been modeled according to the COSMO[25] approach, by considering a polarizable continuum medium characterized by ϵ values of 4 and 40.

To analyze the electronic structure of a system actually composed by two subunits (Fe_4S_4 and $[2Fe]_H$), useful information can be obtained by a consistent representation of the density of states (DOS) projected on different parts of the system, and for different subsets of basis functions. The plots of DOS have been obtained by broadening each energy value of the MO spectrum with a Gaussian function $G(\epsilon_i, \gamma)$, and summing over all the levels corresponding to occupied MOs as

$$\mathrm{DOS} = \sum_{i=1}^{no} G_i(\varepsilon_i, \gamma)$$

γ being the broadening parameter and n_o the number of orbitals. Obviously, for unrestricted wave functions a suitable partition is $\mathrm{DOS} = \mathrm{DOS}_\alpha + \mathrm{DOS}_\beta$, with

$$\mathrm{DOS}_\alpha = \sum_{i=1}^{no(\alpha)} G_i(\varepsilon_i^\alpha, \gamma)$$

$$\mathrm{DOS}_\beta = \sum_{i=1}^{no(\beta)} G_i(\varepsilon_i^\beta, \gamma)$$

When projection of DOS is to be made on a given subset of basis functions (belonging to a specific part of the complex or just identifying a chemically relevant group of orbitals), one can introduce the weight of each basis function, according to the equation

$$\mathrm{DOS}^{\alpha(\beta)} = \sum_{S=1}^{nS} \sum_{i=1}^{no(\alpha)(\beta)} \sum_{j=S} w_{ji} G_i(\varepsilon_i^{\alpha(\beta)}, \gamma)$$

where the w_{ji} coefficients are simply derived from the normalization condition $\sum_{j=1}^{w_{ji}}$, and $w_{ji} = \sum_k \mathbf{C}_{ji}\, \mathbf{C}_{ki}\mathbf{S}_{jk}$, with $\mathbf{C}_i$ the ith MO vector, and $\mathbf{S}$ the overlap matrix.

In the following, atoms will be labeled according to Figure 2. Energies, relevant geometrical parameters, and details of the calculation of exchange coupling constants of the species investigated in this work are reported in the Supporting Information.

Results and Discussion

Preliminary Considerations. As outlined in the Introduction, the nature of the chelating ligand bridging the two iron atoms of the $[2Fe]_H$ subcluster is still controversial (pdt vs dtma). In this study, for the sake of simplicity, and to allow

(25) (a) Klamt, A. *J. Phys. Chem.* **1995**, *99*, 2224. (b) Klamt, A. *J. Phys. Chem.* **1996**, *100*, 3349.

comparison with previous data,[16] we have considered only models featuring pdt as chelating ligand. Indeed, the main goal of this study was the evaluation of the effects of the Fe_4S_4 moiety on the $[2Fe]_H$ subcluster, possibly avoiding concurring effects due to other chemical groups, for which the biochemical relevance is still a matter of debate. In fact, the presence of dtma may confer to the binuclear cluster a richer chemistry due to the two possible protonation states of dtma and to possible interaction of the dtma NH group with the Fe_d ion.[12e] Of course, results obtained for H-cluster models including pdt will be a useful reference for possible future studies of dtma complexes.

The overall charge of $[(CH_3S)_4(Fe_4S_4)(\mu\text{-pdt})(Fe_2)(CO)_3(CN)_2]$ complexes has been set according to the following considerations. In the experimentally characterized forms of the enzyme, the Fe_4S_4 cluster linked to the $[2Fe]_H$ moiety is EPR-silent and therefore in the +2 redox state (hereafter the overall redox state of the cubane will be indicated by the charge of the Fe_4S_4 core).[7] As for the binuclear $[2Fe]_H$ cluster, spectroscopic data indicate that the active oxidized (H_{ox}) and reduced (H_{red}) forms are compatible with [Fe(I), Fe(II)] and [FeI), Fe(I)] redox states, respectively.[6,7,26] Further reduction of H_{red} leads to a super-reduced species (H_{sred}).[27] Therefore, the catalytically active H-cluster in H_{ox} should correspond to the complex $[(CH_3S)_4(Fe_4S_4)(\mu\text{-pdt})(Fe_2)(CO)_3(CN)_2]^{3-}$ (hereafter referred to as $Fe_6S_6]^{3-}$), whereas the H-cluster in the H_{red} and H_{sred} form of the enzyme should correspond to the $[(CH_3S)_4(Fe_4S_4)(\mu\text{-pdt})(Fe_2)(CO)_3(CN)_2]^{4-}$ (hereafter referred to as **$[Fe_6S_6]^{4-}$**) and $[(CH_3S)_4(Fe_4S_4)(\mu\text{-pdt})(Fe_2)(CO)_3(CN)_2]^{5-}$ (hereafter referred to as **$[Fe_6S_6]^{5-}$**) species, respectively.

Compounds with a negative charge as large as −5 are expected to be stable only in condensed phases or in a protein environment, whereas they should lose electrons in the gas phase.[28] Some occupied molecular orbitals can also have unphysical positive eigenvalues.[29] However, it must be noted that the strength of the repulsion between excess electrons is roughly proportional to $Q^2/2r$, where Q is the total charge and r is the average radius of the ion.[30] Consequently, because of the large size of the molecules investigated here, the strength of the repulsion in $[(CH_3S)_4(Fe_4S_4)(\mu\text{-pdt})(Fe_2)(CO)_3(CN)_2]^{5-}$ is similar to that calculated for the $[Fe_4S_4(SCH_3)_4]^{4-}$ cluster or other large highly charged anions, which have been the subject of theoretical investigation.[31] In fact, in spite of these potential problems, as noted by Noodleman et al.,[30] energies and charge distribution of highly charged anions are usually reasonable when environment effects are taken into account. In this work, to keep into account environment effects, we have used the conductor-like screening solvation model (COSMO),[25,32] which has been already shown to mimic satisfactorily the effects of an averaged protein environment on the structural and electronic properties of metal cofactors.[33]

$[(SCH_3)_4(Fe_4S_4)(\mu\text{-pdt})(Fe_2)(CO)_3(CN)_2]^{3-}$. Experimental results converge in describing the H_{ox} form of the enzyme as a μ-CO [Fe(I), Fe(II)]−[2Fe(III), 2Fe(II)] species. Accordingly, we initially studied the H-cluster model $[(CH_3S)_4(Fe_4S_4)(\mu\text{-pdt})(Fe_2)(\mu\text{-CO})(CO)_2(CN)_2]^{3-}$ (**$[Fe_6S_6]b^{3-}$**).

Relevant geometrical parameters of **$[Fe_6S_6]b^{3-}$** optimized in a vacuum (**$[Fe_6S_6]b_1^{3-}$**), and in a polarizable continuum medium characterized by ϵ values = 4 (**$[Fe_6S_6]b_4^{3-}$**) and 40 (**$[Fe_6S_6]b_{40}^{3-}$**), are collected in Table S1 of the Supporting Information. The structural features of the $[2Fe]_H$ cluster in **$[Fe_6S_6]b_1^{3-}$** fit reasonably well with experimental data and previous calculations.[3−5,16,17] In particular, the Fe_p-Fe_d distance (2.56 Å) is only 0.01 Å shorter than the experimental value reported in ref 4, which probably corresponds to a mixture of the H_{ox} and H_{red} forms of the enzyme (Table S1 in the Supporting Information).[34] However, a noticeable exception is observed for the $Fe_1-S_b-Fe_p$ angle (137 ± 1°; Figure 2 for atom labels), which is more than 20° larger than the corresponding experimental value.[35] Interestingly, the $Fe_1-S_b-Fe_p$ angle is strongly affected by the value of the dielectric constant. In fact, it decreases from 137 ± 1° to 125 ± 2°, when going from **$[Fe_6S_6]b_1^{3-}$** to **$[Fe_6S_6]b_{40}^{3-}$**. The value in **$[Fe_6S_6]b_{40}^{3-}$** is much closer to the X-ray diffraction data (Table S1 in the Supporting Information)[36] and also very close to the Fe−S−Fe angle between the Fe_4S_4 cluster

(26) Liu, X.; Ibrahim, S. K.; Tard, C.; Pickett, C. J. *Coord. Chem. Rev.* **2005**, *249*, 1641.

(27) Roseboom, W.; De Lacey, A. L.; Fernandez, V. M.; Hatchikian, E. C.; Albracht, S. P. J. *J. Biol. Inorg. Chem.* **2006**, *11*, 102.

(28) The ionization potential (IP) of $[(CH_3S)_4(Fe_4S_4)(m\text{-pdt})(Fe_2)(m\text{-CO})(CO)_2(CN)_2]^{5-}$ is negative and as large as −7.12 eV, indicating an unstable system. Nevertheless, such a redox state can be computed despite its tendency to lose an electron because of the finite nature of the basis set, which cannot represent the continuum electron and consequently confines electrons in a metastable state.

(29) Calculations performed enclosing the H-cluster in a positively charged spherical cage, which produces a shift of all of the occupied orbital energies to negative values, without significantly affecting the molecular geometry and the electron distribution (data not shown).

(30) Noodleman, L.; Peng, C. Y.; Case, D. A.; Mouesca, J.-M. *Coord. Chem. Rev.* **1995**, *144*, 199.

(31) (a) Torres, R. A.; Lovell, T.; Noodleman, L.; Case, D. A. *J. Am. Chem. Soc.* **2003**, *125*, 1923. (b) Amara, P.; Volbeda, A.; Fontecilla-Camps, J. C.; Field, M. J. *J. Am. Chem. Soc.* **2005**, *127*, 2776.

(32) COSMO has been shown to give accurate results when the quantum cluster charge and polarity is not too high. Again, we have to highlight that the large negative charge of the compounds investigated here is spread over a large volume due to the size of the molecule. In fact, the apparent surface charge (ASC) generated for each tessera of the cavity surface is even smaller than that generated for less-charged smaller anions (data not shown).

(33) Zampella, G.; Fantucci, P.; Pecoraro, V.; De Gioia, L. *J. Am. Chem. Soc.* **2005**, *127*, 953.

(34) The redox states of the H-cluster in the X-ray structures have not been unambiguously assigned. Theoretical and experimental results suggest that the structure of ref 3 corresponds to the fully oxidized H_{inact} form of the enzyme, the structure of ref 4 corresponds to a mix of H_{ox} and H_{red} states, and the structure of ref 5 is entirely assigned to the H_{red} form of the enzyme. The structure of ref 5 is not available in the PDB, and only the distances reported in Table 1 are given in the original publication. In parenthesis are the distances of the second non-crystallographically related molecule.

(35) The Fe_d coordination environment in the enzyme is square pyramidal, whereas a trigonal bypiramidal arrangement, with one sulfur atom of the PDT group and one CO ligand in axial positions, is observed in $[Fe_6S_6]b_1^{3-}$ (Supporting Information). This arrangement brings the CN ligand coordinated to the Fe_d atom in the plane defined by the two iron atoms and one sulfur atom of the PDT group, a position which differs significantly from that observed experimentally. A similar arrangement of the $Fe_d(CO)_2(CN)$ group is found in the binuclear complex $[Fe_2S_2(H)]b_1^{1-}$, in which the Fe_4S_4 cluster is replaced by the CH_3SH group, whereas in the case of $[Fe_2S_2]b_1^{2-}$ the coordination geometry of the Fe_d atom is more similar to the X-ray structure.

(36) The Fe_d atom in $[Fe_6S_6]b_4^{3-}$ and in $[Fe_6S_6]b_{40}^{3-}$, as well as in the binuclear model complexes $[Fe_2S_2(H)]b_{4-40}^{1-}$ and $[Fe_2S_2]b_{4-40}^{2-}$ assumes a square pyramidal configuration, with the CN ligand moving in the plane defined by the two sulfur atoms of PDT and the equatorial CO, as observed in the enzyme.

Table 1. Atomic Spin Densities and Atomic Charges of the Iron Atoms in the H-Cluster Models Computed at BP86/def-TZVP Level of Theory[a]

		$[Fe_6S_6]b^{3-}$	$[Fe_6S_6]t^{3-}$	$[Fe_6S_6]b^{4-}$	$[Fe_6S_6]t^{4-}$	$[Fe_6S_6]b^{5-}$	$[Fe_6S_6]t^{5-}$
				Atomic Spin Densities			
$Fe_{1,2}$	$\epsilon = 1$	3.13*,3.09	3.11*,3.10	3.11*,3.09	3.09*,3.08	[b]	3.34*, 3.26
	$\epsilon = 4$	3.10*,3.07	3.07*,3.07	3.04*,3.06	3.04*,3.07	3.24*, 3.21	3.24*, 3.22
	$\epsilon = 40$	3.08*,3.06	3.08*,3.07	3.05*,3.05	3.04*,3.07	3.21*, 3.20	[c]
$Fe_{3,4}$	$\epsilon = 1$	−3.12,−3.10	−3.13,−3.10	−3.21,−3.21	−3.20,−3.22	[b]	−3.01, −3.00
	$\epsilon = 4$	−3.08,−3.07	−3.09,−3.06	−3.14,−3.13	−3.12,−3.15	−2.89, −2.91	−2.93, −2.89
	$\epsilon = 40$	−3.06,−3.05	−3.06,−3.06	−3.09,−3.11	−3.09,−3.12	−2.87, −2.87	[c]
Fe_p	$\epsilon = 1$	0.04	1.23	0.03	0.45	[b]	0.05
	$\epsilon = 4$	0.17	1.21	0.04	0.21	0.01	0.03
	$\epsilon = 40$	0.20	0.95	0.02	0.12	0.01	[c]
Fe_d	$\epsilon = 1$	0.97	−0.09	0.31	−0.04	[b]	0.00
	$\epsilon = 4$	0.88	−0.09	0.17	0.01	0.03	0.01
	$\epsilon = 40$	0.84	0.00	0.16	0.02	0.02	[c]
				Atomic Charges			
$Fe_{1,2}$	$\epsilon = 1$	0.21*,0.17	0.19*,0.17	0.22*,0.20	0.21*,0.20	[b]	0.29*, 0.25
	$\epsilon = 4$	0.23*,0.15	0.22*,0.15	0.23*,0.16	0.18*,0.17	0.28*, 0.22	0.28*, 0.22
	$\epsilon = 40$	0.26*,0.13	0.23*,0.14	0.25*,0.14	0.22*,0.14	0.30*, 0.19	[c]
$Fe_{3,4}$	$\epsilon = 1$	0.18,0.17	0.18,0.17	0.22,0.21	0.21,0.21	[b]	0.25, 0.26
	$\epsilon = 4$	0.15,0.15	0.15,0.15	0.17,0.17	0.17,0.18	0.20, 0.19	0.19, 0.20
	$\epsilon = 40$	0.13,0.14	0.14,0.14	0.15,0.15	0.16,0.15	0.16, 0.16	
Fe_p	$\epsilon = 1$	−0.47	−0.29	−0.42	−0.32	[b]	−0.27
	$\epsilon = 4$	−0.49	−0.32	−0.43	−0.31	−0.40	−0.28
	$\epsilon = 40$	−0.51	−0.32	−0.43	−0.27	−0.40	[c]
Fe_d	$\epsilon = 1$	−0.43	−0.55	−0.44	−0.53	[b]	−0.52
	$\epsilon = 4$	−0.42	−0.55	−0.42	−0.52	−0.42	−0.52
	$\epsilon = 40$	−0.40	−0.55	−0.41	−0.51	−0.41	[c]
$q_{Fe_4S_4}$[d]	$\epsilon = 1$	−1.55	−1.59	−2.00	−1.99	[b]	−2.65
	$\epsilon = 4$	−1.51	−1.51	−1.83	−1.82	−2.61	−2.60
	$\epsilon = 40$	−1.49	−1.51	−1.73	−1.78	−2.59	[c]

[a] $Fe_{1,2}$ and $Fe_{2,3}$ refer to the iron atoms of the two layers coupled antiferromagnetically in the **$[Fe_4S_4]$** cluster; Fe_p and Fe_d refer to the proximal and distal iron atoms of the $[2Fe]_H$ cluster, respectively (the iron atom of the $[Fe_4S_4]$ cluster linked to the sulfur atom bridging the $[Fe_4S_4]$ and the $[2Fe]_H$ clusters is labeled with an asterisk). [b] Not available because the structure does not correspond to a stationary point on the potential energy surface. [c] Not available because the geometry optimization converges to the bridged form. [d] Net charge of the $\{Fe_4S_4(CH_3S)_4\}$ moiety in the H-cluster.

and the siroheme iron in sulfite reductase (126°),[37] indicating that the averaged description of the protein environment adopted in our calculations is adequate to reproduce this important structural feature.

The geometrical parameters of the Fe_4S_4 cluster in **$[Fe_6S_6]b_1^{3-}$** are in good agreement with experimental data (Table S1 in the Supporting Information). In addition, the structure of the cubane in the H-cluster is nearly identical to that calculated for the **$[Fe_4S_4(CH_3S)_4]^{2-}$** (hereafter referred to as $[Fe_4S_4]^{2-}$) complex in the same environment (Table S40 in the Supporting Information), indicating that the $[2Fe]_H$ cluster does not affect the molecular geometry of the Fe_4S_4 unit in **$[Fe_6S_6]b^{3-}$**. Likewise, the Fe_4S_4 cluster does not affect significantly the structure of the $[2Fe]_H$ cluster, as deduced from the comparison of the geometry of **$[Fe_6S_6]b^{3-}$** with that of the bimetallic complexes $[(SHCH_3)(\mu\text{-pdt})(\mu\text{-CO})(Fe_2)(CO)_2(CN)_2]^{1-}$ and $[(SCH_3)(\mu\text{-pdt})(\mu\text{-CO})(Fe_2)(CO)_2(CN)_2]^{2-}$ (hereafter referred to as **$[Fe_2S_2(H)]^{1-}$** and **$[Fe_2S_2]^{2-}$**, respectively), in agreement with previous calculations (Table S32 in the Supporting Information).[16]

In **$[Fe_6S_6]b_1^{3-}$**, **$[Fe_6S_6]b_4^{3-}$**, and **$[Fe_6S_6]b_{40}^{3-}$**, the unpaired electron is localized on the Fe_d atom of the $[2Fe]_H$ cluster (Table 1), in agreement with experimental data and previous calculations.[7,16,17] The theoretical exchange coupling constant J_{cube} is 391 ± 5 cm^{-1} in **$[Fe_6S_6]b_1^{3-}$**, and it increases to 419 ± 4 cm^{-1} in **$[Fe_6S_6]b_{40}^{3-}$** (Table 2). These values are very similar to those calculated for the **$[Fe_4S_4]^{2-}$** cluster in the same environment (Table S41 in the Supporting Information), indicating that the $[2Fe]_H$ subcluster does not affect the electronic properties of the Fe_4S_4 moiety in **$[Fe_6S_6]b^{3-}$**.

Table 2. Exchange Coupling Parameters, J_{cube}, J_H, and B' (cm^{-1}) Computed at the RI-BP86/def-TZVP Level of Theory (in Parentheses are the Values Calculated for the Corresponding $[Fe_4S_4(SCH_3)]^{-x}$ ($x = -2, -3$) Model Complexes)

	B'	J_{cube}	J_H
$[Fe_6S_6]b_1^{3-}$		391 ± 5 (426)[a]	3 ± 1
$[Fe_6S_6]b_4^{3-}$		409 ± 3 (436)[a]	22 ± 7
$[Fe_6S_6]b_{40}^{3-}$		419 ± 4 (432)[a]	29 ± 4
$[Fe_6S_6]t_1^{3-}$		355 ± 5 (426)[a]	73 ± 9
$[Fe_6S_6]t_4^{3-}$		399 ± 5 (436)[a]	164 ± 17
$[Fe_6S_6]t_{40}^{3-}$		411 ± 4 (432)[a]	147 ± 40
$[Fe_6S_6]b_1^{4-}$		310 ± 5 (426)[a]	
$[Fe_6S_6]b_4^{4-}$		358 ± 5 (436)[a]	
$[Fe_6S_6]b_{40}^{4-}$		395 ± 8 (432)[a]	
$[Fe_6S_6]t_1^{4-}$		328 ± 9 (426)[a]	
$[Fe_6S_6]t_4^{4-}$		382 ± 7 (436)[a]	
$[Fe_6S_6]t_{40}^{4-}$		391 ± 6 (432)[a]	
$[Fe_6S_6]b_4^{5-}$	536 (629)[b]	360 ± 9 (390)[b]	
$[Fe_6S_6]b_{40}^{5-}$	556 (640)[b]	376 ± 6 (394)[b]	
$[Fe_6S_6]t_1^{5-}$	538 (601)[b]	315 ± 12 (356)[b]	
$[Fe_6S_6]t_4^{5-}$	559 (629)[b]	354 ± 29 (390)[b]	

[a] Value calculated for the **$[Fe_4S_4(SCH_3)]^{-2}$** (**$[Fe_4S_4]^{2-}$**) complex. [b] Value calculated for the **$[Fe_4S_4(SCH_3)]^{-3}$** (**$[Fe_4S_4]^{3-}$**) complex.

In **$[Fe_6S_6]b_1^{3-}$**, the energies of the ferromagnetic BS_1 and antiferromagnetic BS_2 solutions are very similar. Consequently, the value of the theoretical exchange coupling constant J_H is only 3 ± 1 cm^{-1}. The J_H value increases to 22 ± 7 and 30 ± 4 cm^{-1} in **$[Fe_6S_6]b_4^{3-}$** and **$[Fe_6S_6]b_{40}^{3-}$** (Table 2), with the latter values being in good agreement with experimental data.[7]

(37) Crane, B. R.; Siegel, L. M.; Getzoff, D. *Science* **1995**, *270*, 59.

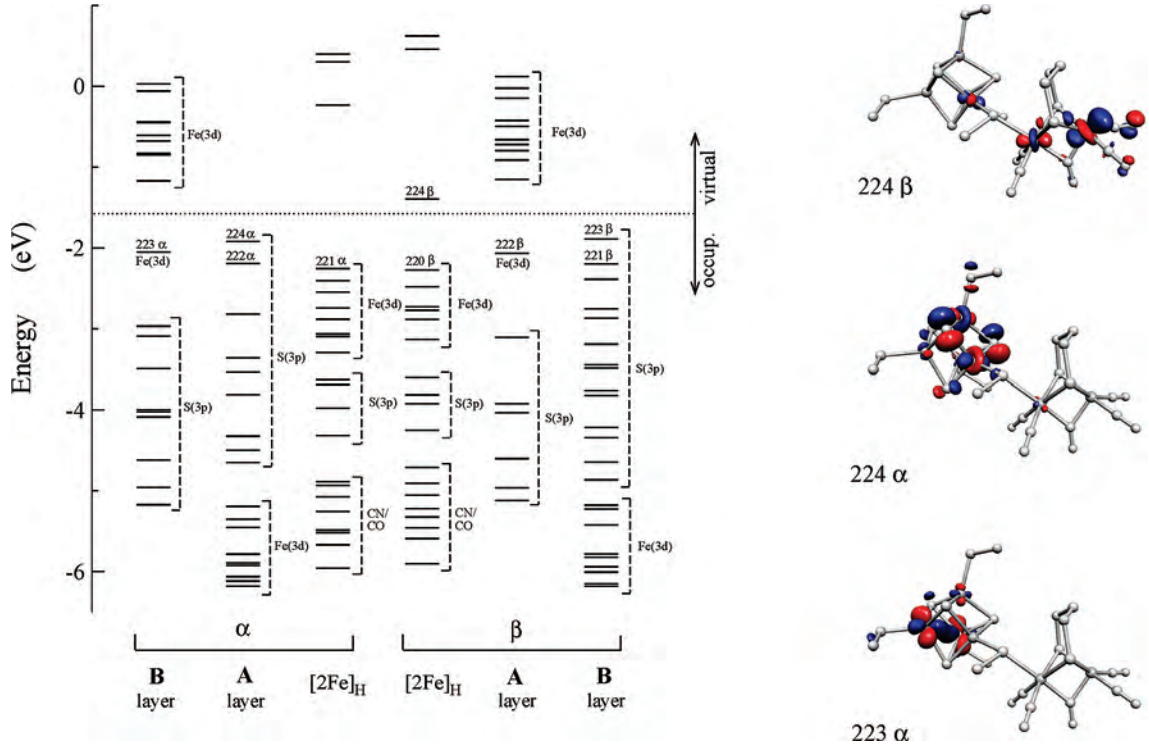

Figure 3. Detailed orbital diagram of the BS_1 state of $[Fe_6S_6]b_4^{3-}$ calculated at the BP86/def-TZVP level of theory. The orbitals are separated horizontally according to their localization in the molecule, and their spin, as indicated in the bottom of the Figure. Starting from the left to the middle are the energies of the orbitals with α spin localized on Fe_2S_2 layers **B** and **A**, and on the $[2Fe]_H$ cluster (Figure 2 for labels). From the middle to the right are the orbitals with β spin of the $[2Fe]_H$ cluster, and of layers **A** and **B**. The horizontal broken line divides occupied (below) and virtual orbitals (above). The energy levels are grouped vertically on the basis of the characteristics of the corresponding orbitals. Some orbitals are partly delocalized on the entire H-cluster. Therefore, the energy level scheme is qualitative. The levels labeled Fe(3d) localized on the Fe_4S_4 cluster correspond to majority spin−orbitals (bottom) and minority spin−orbitals (top). The levels labeled S(3p) correspond to 3p orbitals of the sulfur atoms, which lie between majority and minority Fe(3d) spin−orbitals. For the $[2Fe]_H$ cluster, levels labeled Fe(3d), S(3p), and CN/CO correspond to 3d orbitals of iron atoms, 3p orbitals of sulfur atoms, and π orbitals or lone pairs of the CO and CN ligand, respectively. On the right, the isodensity surface of some relevant MOs are also shown. In particular, orbital **224*β*** is the lowest unoccupied β orbital, and it is the d_{z^2} orbital of the Fe_d atom; **224α** is the highest occupied α orbital localized on the **A** layer of the Fe_4S_4 cluster; **223α** is the Fe−Fe bonding minority spin−orbital filled with the mixed valence electron, and fully delocalized between the two iron atoms of the **B** layer.

The net charge of the $\{(CH_3S)_4(Fe_4S_4)\}$ moiety in $[Fe_6S_6]b^{3-}$ is about −1.5, a value that, when compared to the overall −2 charge of the isolated $[(CH_3S)_4(Fe_4S_4)]^{2-}$ cluster, shows that a significant charge transfer (about 0.5 electrons) takes place from the Fe_4S_4 moiety to the $[2Fe]_H$ cluster. This observation is relevant because it is known that μ-CO forms of the $[2Fe]_H$ cluster are stabilized when electron donor groups are coordinated to Fe_p.[13,14] The extent of the charge transfer computed in the H-cluster is intermediate between that calculated from the SCH_3^- (0.65) and $SHCH_3$ (0.25) groups to the Fe_2S_2 unit in the bimetallic complexes $[Fe_2S_2]b^{2-}$ and $[Fe_2S_2(H)]b^{1-}$, respectively.

The electronic structure of $[Fe_6S_6]b^{3-}$ was further investigated by analyzing the orbital diagram shown in Figure 3. As expected, in $[Fe_6S_6]b_1^{3-}$ some occupied MOs have positive energy values because of the large negative charge of the system. The orbital diagrams for $[Fe_6S_6]b_4^{3-}$ and $[Fe_6S_6]b_{40}^{3-}$ are qualitatively similar to that computed for $[Fe_6S_6]b_1^{3-}$, but the presence of the polarizable continuum medium shifts all orbital energies to negative values. This observation holds true for all of the complexes investigated, and therefore, for the sake of brevity, in the following, the orbital diagrams will be explicitly discussed only for $\epsilon = 4$. In $[Fe_6S_6]b_4^{3-}$, the Fe_4S_4 cluster is characterized by the so-called inverted scheme,[30,38] with the majority spin Fe(3d) orbitals of each Fe_2S_2 layer lower in energy than the S(3p) orbitals. On the contrary, in the $[2Fe]_H$ cluster the Fe(3d) orbitals lie at higher energies relative to the S(3p) orbitals, as expected for a normal level scheme.

A more rigorous representation of the electronic structure is provided by DOS profiles projected on a selected groups of atoms, for which the contribution to each MO of these atoms can be quantitatively evaluated. The DOS profile projected on the Fe_4S_4 cluster (Figure S1 in the Supporting Information) shows that Fe(3d) orbitals contribute to the energy levels along the entire profile.[39] In particular, even though the DOS profile can be clearly assigned to the inverted scheme, the contribution from Fe(3d) and S(3p) orbitals to the energy levels is significantly more mixed than that predicted from simple ligand field arguments, as could be expected due to the high covalency of the Fe−S bonds. In the $[2Fe]_H$ cluster, Fe(3d) orbitals contribute only to the higher energy levels (−2/−3.5 eV), whereas S(3p) orbitals and lone pairs of the nitrogen atoms are at lower energies (Figure S1 in the Supporting Information).

As shown in the orbital diagram of Figure 3, the three occupied α and β molecular orbitals of highest energy in $[Fe_6S_6]b_4^{3-}$ are localized on the Fe_4S_4 cluster. Interestingly,

(38) (a) Aizman, A.; Case, D. A. *J. Am. Chem. Soc.* **1982**, *104*, 3269. (b) Noodleman, L.; Baerends, E. J. *J. Am. Chem. Soc.* **1984**, *106*, 2316. (c) Noodleman, L.; Case, A., D. *Adv. Inorg. Chem.* **1992**, *38*, 423.

the lowest-unoccupied β orbital in **[Fe$_6$S$_6$]b$_4^{3-}$** is localized on the [2Fe]$_H$ cluster, and corresponds to the d_{z^2} orbital of the Fe$_d$ atom. This unoccupied orbital is close in energy to the highest occupied α and β orbitals, and it might be involved in the binding of H_2 to the Fe$_d$ atom. Furthermore, the energy gap between the lowest unoccupied β orbital and the highest occupied orbitals in **[Fe$_6$S$_6$]b^{3-}** decreases significantly as the dielectric constant increases ($\Delta E = 0.79$, 0.52, and 0.45 eV for $\epsilon = 1$, 4, and 40, respectively). It is also interesting to note that in **[Fe$_6$S$_6$]b$_1^{3-}$** the unoccupied d_{z^2} orbital of Fe$_d$ is slightly higher in energy than an unoccupied β orbital localized on the Fe_4S_4 cluster, whereas the opposite is true in **[Fe$_6$S$_6$]b$_4^{3-}$** and **[Fe$_6$S$_6$]b$_{40}^{3-}$**. As it will be discussed below, this observation is relevant for the reduction of **[Fe$_6$S$_6$]b^{3-}**, in which the added electron will occupy one of these orbitals.

The $[(CH_3S)_4(Fe_4S_4)(\mu\text{-pdt})(Fe_2)(CO)_3(CN)_2]^{3-}$ isomer featuring all terminal COs (**[Fe$_6$S$_6$]t^{3-}**) has been investigated because of its similarity with $Fe_2(L)_6$ synthetic complexes and with the species transiently observed upon irradiation of the CO-inhibited form of the enzyme.[40]

In **[Fe$_6$S$_6$]t$_1^{3-}$**, the Fe$_d$ and Fe$_p$ atoms are in a distorted square pyramidal arrangement. As noted for **[Fe$_6$S$_6$]b^{3-}**, the environment affects the structural properties of **[Fe$_6$S$_6$]t^{3-}** (Table S1 in the Supporting Information). In particular, the Fe$_1$−S$_b$−Fe$_p$ angle and the S$_b$−Fe$_p$ bond length decrease by about 20° and 0.1 Å, respectively, going from **[Fe$_6$S$_6$]t$_1^{3-}$** to **[Fe$_6$S$_6$]t$_{40}^{3-}$**.[41] The structure of the Fe_4S_4 cluster is nearly identical to that calculated for **[Fe$_4$S$_4$]$^{2-}$**.

In **[Fe$_6$S$_6$]t^{3-}**, the unpaired electron is fully localized on the Fe$_p$ atom (Table 1). This means that movement of a CO ligand from bridging (**[Fe$_6$S$_6$]b^{3-}**) to terminal (**[Fe$_6$S$_6$]t^{3-}**) position is accompanied by a spin transfer from Fe$_d$ to Fe$_p$. A similar behavior was also observed in the binuclear complexes $[(SCH_3)(\mu\text{-pdt})(Fe_2)(CO)_3(CN)_2]^{2-}$ (**[Fe$_2$S$_2$]t^{2-}**) and $[(SCH_3)(\mu\text{-pdt})(Fe_2)(CO)_3(CN)_2]^{1-}$ (**[Fe$_2$S$_2$(H)]t^{1-}**). Therefore, the observed spin transfer is peculiar for the [2Fe]$_H$ cluster, and it is not affected by the presence of the Fe_4S_4 cluster.

The exchange coupling constant J_{cube} calculated for **[Fe$_6$S$_6$]t$_1^{3-}$** is 355 ± 5 cm^{-1} and increases to 411 ± 4 cm^{-1} in **[Fe$_6$S$_6$]t$_{40}^{3-}$** (Table 2). These values are slightly smaller than those calculated for **[Fe$_6$S$_6$]b^{3-}**, indicating that the [2Fe]$_H$ subunit in **[Fe$_6$S$_6$]b^{3-}** more strongly affects the magnetic exchange properties of the cubane. The exchange interaction between the two clusters is expected to be significantly larger than that in **[Fe$_6$S$_6$]b^{3-}** due to localization of the spin on the Fe$_p$ atom, which is adjacent to the Fe_4S_4 cluster. Indeed, the average value of J_H calculated for **[Fe$_6$S$_6$]t$_1^{3-}$** is about 70 cm^{-1}, a value about one order of magnitude larger than in **[Fe$_6$S$_6$]b$_1^{3-}$**. Also in this case the environment strongly affects J_H, which increases to about 150 cm^{-1} when $\epsilon = 40$.

The charge transferred from the $\{(CH_3S)_4(Fe_4S_4)\}$ moiety to the [2Fe]$_H$ cluster in **[Fe$_6$S$_6$]t^{3-}** ($\sim$0.5) is similar to that calculated for **[Fe$_6$S$_6$]b^{3-}** (Table 1). The orbital diagram and DOS profiles (not shown) computed for **[Fe$_6$S$_6$]t$_4^{3-}$** are also similar to those discussed for **[Fe$_6$S$_6$]b$_4^{3-}$**.

The energies of **[Fe$_6$S$_6$]t^{3-}** and **[Fe$_6$S$_6$]b^{3-}**, not corrected with spin projection techniques,[42] are nearly identical (the energy difference being always within 1 kcal mol^{-1}, Table S2 in the Supporting Information), suggesting that the two isomers can coexist at room temperature. It is interesting to note that the computed energy difference is in between those calculated for the bimetallic complexes, in which Fe_4S_4 is replaced by SCH_3^- and $SHCH_3$ (Supporting Information).

$[(SCH_3)_4(Fe_4S_4)(\mu\text{-pdt})(Fe_2)(CO)_3(CN)_2]^{4-}$. Monoelectron reduction of **[Fe$_6$S$_6$]$^{3-}$** leads to $[(SCH_3)_4Fe_4S_4(\mu\text{-pdt})Fe_2(CO)_3(CN)_2]^{4-}$ (**[Fe$_6$S$_6$]$^{4-}$**), which corresponds to the diamagnetic H_{red} state of the enzyme. Also in this case both structures featuring a μ-CO (**[Fe$_6$S$_6$]b^{4-}**) and all-terminal CO groups (**[Fe$_6$S$_6$]t^{4-}**) correspond to stationary points on the potential energy hypersurface.

In the μ-CO isomer **[Fe$_6$S$_6$]b$_1^{4-}$**, the Fe$_p$−Fe$_d$ distance is 2.62 ± 0.00 Å, a value significantly larger than that observed in the crystallographic structure assigned to the H_{red} form of the enzyme (Table S1 in the Supporting Information).[5,34] The Fe$_1$−S$_b$−Fe$_p$ angle is about 150°, a value more than 30° larger than in the X-ray structure. The μ-CO ligand asymmetrically bridges the two iron atoms (Fe$_p$−C(O) = 2.04 ± 0.01 Å and Fe$_d$−C(O) = 1.85 ± 0.01 Å), moving toward Fe$_d$ with respect to **[Fe$_6$S$_6$]b$_1^{3-}$**.

When **[Fe$_6$S$_6$]b^{4-}** is optimized in a polarizable continuum medium (**[Fe$_6$S$_6$]b$_4^{4-}$** and **[Fe$_6$S$_6$]b$_{40}^{4-}$**), the Fe$_p$−Fe$_d$ distance and the Fe$_1$−S$_b$−Fe$_p$ angle approach the experimental values (Table S1). The μ-CO further moves away from the Fe$_p$ atom (Fe$_p$−C(O) = 2.07 ± 0.01 in **[Fe$_6$S$_6$]b$_{40}^{4-}$**). Nevertheless, in **[Fe$_6$S$_6$]b$_{40}^{4-}$** the Fe$_p$−C(O) distance remains significantly shorter than in the X-ray structure (Fe$_p$−C(O) $\approx$ 2.5 Å).

The structure of the [2Fe]$_H$ cluster in **[Fe$_6$S$_6$]b^{4-}** is fairly similar to that calculated for the $[(SCH_3)(\mu\text{-pdt})(Fe_2)(CO)_3(CN)_2]^{3-}$ (**[Fe$_2$S$_2$]b^{3-}**) and $[(SHCH_3)(\mu\text{-pdt})(Fe_2)(CO)_3(CN)_2]^{2-}$ (**[Fe$_2$S$_2$(H)]b^{2-}**) complexes (Tables S1 and S33 in the Supporting Information).

Even though **[Fe$_6$S$_6$]b^{4-}** is diamagnetic, analysis of spin populations (Table 1) reveals that in **[Fe$_6$S$_6$]b$_1^{4-}$** the Fe$_d$ atom is still characterized by a significant positive spin density (0.31), whereas the corresponding negative spin density is localized on the Fe_4S_4 cluster. The net charge calculated for the $\{(CH_3S)_4(Fe_4S_4)\}$ moiety in **[Fe$_6$S$_6$]b$_1^{4-}$** is −2.0, indicat-

(39) In fact, in addition to the two broad peaks in the region −6/−5 eV, assigned to the majority spin Fe(3d) orbitals, several other peaks at higher energies are observed. The peaks assigned to S(3p) orbitals are also distributed along the entire DOS profile. In particular, two intense peaks assigned to S* (3p) orbitals occur in the same region of the majority spin Fe(3d) orbitals (−6/−5 eV), whereas S_{cys}(3p) orbitals mainly contribute to the energy levels in two regions centered at about −4.0 and −3.0 eV.

(40) Chen, Z.; Lemon, B. J.; Huang, S.; Swartz, D. J.; Peters, J. W.; Bagley, K. A. *Biochemistry* **2002**, *41*, 2036.

(41) The large standard deviation observed in the case of the S$_b$−Fe$_p$ distance (Tables, S4, S5, and S6 in the Supporting Information) is due to the different lengths calculated for the ferromagnetic BS$_1$ and antiferromagnetic BS$_2$ states. Indeed, the S$_b$−Fe$_p$ bond length in the BS$_2$ state is about 0.04 Å shorter than that in BS$_1$ state.

(42) As discussed in Computational Details, BS states are not pure spin states. Correspondingly, the energy of a BS state does not correspond to the energy of the ground state of the molecule. However, the ground-state energy can be obtained by using spin-projection techniques.

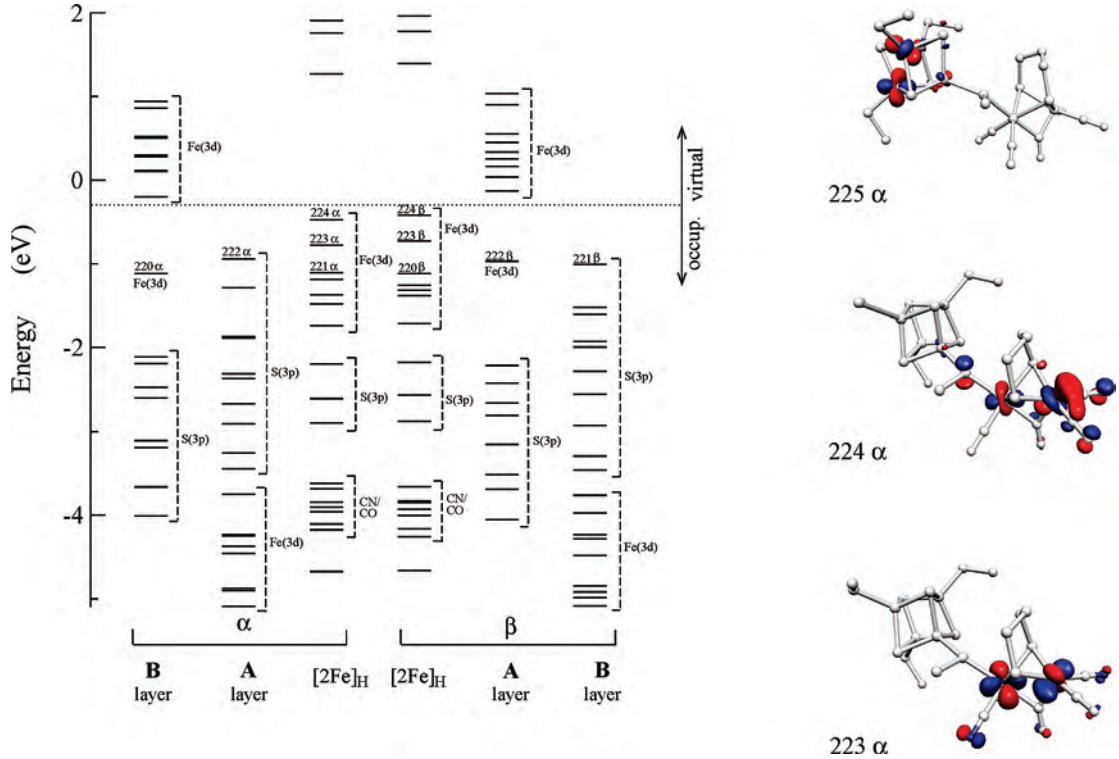

Figure 4. Detailed orbital diagram of the BS_1 state $[Fe_6S_6]b_4^{4-}$. The labels and the description of the diagram have been given in the caption of Figure 2. On the right, the isodensity surfaces of some relevant MOs are also shown. In particular, orbital **225α** is the first unoccupied α orbital, localized on the **B** layer of the Fe_4S_4 cluster, and orbitals **224α** and **223α** are the first and second highest occupied α orbitals, respectively, both localized on the $[2Fe]_H$ cluster.

ing that in the reduction from $[Fe_6S_6]b_1^{3-}$ to $[Fe_6S_6]b_1^{4-}$ the negative charge of the cubane increases by about 0.5 electrons (Table 1). The spin and charge density values are compatible with partial reduction of both the Fe_4S_4 and $[2Fe]_H$ clusters and therefore with delocalization over the entire H-cluster of the electron added in the $[Fe_6S_6]b_1^{3-} + e^- \rightarrow [Fe_6S_6]b_1^{4-}$ reduction.

In $[Fe_6S_6]b_4^{4-}$ and $[Fe_6S_6]b_{40}^{4-}$, the spin density on the $[2Fe]_H$ cluster is progressively removed (Table 1), and correspondingly the negative charge of the $\{(CH_3S)_4(Fe_4S_4)\}$ moiety becomes −1.8 and −1.7, respectively. Therefore, the electron added to $[Fe_6S_6]b^{3-}$ becomes completely localized on the $[2Fe]_H$ cluster in $[Fe_6S_6]b_4^{4-}$ and $[Fe_6S_6]b_{40}^{4-}$, which consequently can be described as [Fe(I), Fe(I)]−[2Fe(III), 2Fe(II)] species.

The computed exchange coupling constant J_{cube} in $[Fe_6S_6]b_1^{4-}$ is 310 ± 5 cm^{-1}, a value significantly smaller than in $[Fe_6S_6]b_1^{3-}$, but that accounts for the partial reduction of the Fe_4S_4 cluster discussed above (Table 2). The value of J_{cube} increases significantly in $[Fe_6S_6]b_4^{4-}$ and $[Fe_6S_6]b_{40}^{4-}$, and for the latter the computed value (395 ± 8 cm^{-1}) is very similar to that calculated for $[Fe_6S_6]b_{40}^{3-}$, further confirming that the Fe_4S_4 cluster in $[Fe_6S_6]b_{40}^{4-}$ is in the oxidized state.

The orbital diagram of $[Fe_6S_6]b_4^{4-}$, shown in Figure 4, differs significantly from that of $[Fe_6S_6]b_4^{3-}$.[43] The reduction of $[Fe_6S_6]b^{3-}$ to give $[Fe_6S_6]b^{4-}$ strongly destabilizes the orbitals localized on the $[2Fe]_H$ cluster, which become higher in energy relative to the orbitals on the Fe_4S_4 cluster. As a consequence, the highest occupied α and β orbitals of $[Fe_6S_6]b_4^{4-}$ are localized on the Fe_d atom of the $[2Fe]_H$ cluster and can be involved in proton binding. As shown in Figure 4, the lowest unoccupied α and β orbitals are localized on the Fe_4S_4 cluster. The energy gap between highest occupied and lowest unoccupied α and β orbitals in $[Fe_6S_6]b_1^{4-}$ is as small as 0.2 eV, and it increases to about 0.3 and 0.4 eV in $[Fe_6S_6]b_4^{4-}$ and $[Fe_6S_6]b_{40}^{4-}$, respectively. This very small energy gap and its dependence on the dielectric constant of the environment explains the delocalization of the β electron observed in $[Fe_6S_6]b_1^{4-}$ as well as its progressive localization on the $[2Fe]_H$ cluster observed in $[Fe_6S_6]b_4^{4-}$ and $[Fe_6S_6]b_{40}^{4-}$.[44] The results discussed above suggest also that specific modifications of the environment may easily invert the order of stability of these frontier orbitals, possibly triggering electron transfer between the $[2Fe]_H$ and the Fe_4S_4clusters.[45]

In $[(SCH_3)_4Fe_4S_4(\mu\text{-pdt})Fe_2(CO)_3(CN)_2]^{4-}$ ($[Fe_6S_6]t_1^{4-}$), the Fe_p and Fe_d atoms are in a distorted square pyramidal arrangement, in which the $Fe_d(CO)_2(CN)$ moiety is slightly

(43) Also, the DOS profile of $[Fe_6S_6]b_4^{4-}$ clearly differs from that of $[Fe_6S_6]b_4^{3-}$ in the region near the Fermi level. In fact, for the former, the DOS at the Fermi level is entirely assigned to the $[2Fe]_H$ cluster, whereas the contribution of Fe_4S_4 falls to zero (part c of Figure 3, panels II and III). The opposite holds true for $[Fe_6S_6]b_4^{3-}$. The DOS profile of the Fe_4S_4 cluster in $[Fe_6S_6]b_4^{4-}$ differs from that of $[Fe_6S_6]b_4^{3-}$ also at lower energies, probably due to its partial reduction.

(44) The near degeneracy of highest occupied and lowest unoccupied orbitals may suggest that the triple state ($S = 1$) could be more stable than the singlet one ($S = 0$). However, the calculated energy of the triplet state in its optimum geometry is larger than that of the singlet.

(45) As an example, protonation of a cysteine sulfur atom coordinated to the Fe_4S_4 results in electron transfer from the $[2Fe]_H$ moiety to the cubane, leading to a species in which the Fe_4S_4 cluster is in the fully reduced state [1Fe(III), 3Fe(II)], the $[2Fe]_H$ moiety is in the oxidized state [Fe(I), Fe(II)], and the two unpaired electrons are antiferromagnetically coupled (data not shown).

rotated, and a CO group approaches the Fe_p atom at a distance of 3.32 ± 0.02 Å (Table S1 in the Supporting Information). Again, the environment affects the molecular and electronic structure of the H-cluster; in particular, the $Fe_1-S_b-Fe_p$ angle decreases from 150 ± 3° in **[Fe$_6$S$_6$]t$_1$$^{4-}$** to 124 ± 2° in **[Fe$_6S_6$]t$_{40}$$^{4-}$** (Table S1 in the Supporting Information). The rotation of the $Fe_d(CO)_2(CN)$ group in **[Fe$_6$S$_6$]t$_{40}$$^{4-}$** leads to a distorted trigonal bipyramidal geometry in which a CO ligand further approaches the Fe_p atom ($Fe_p-C(O)$ = 3.13 ± 0.01 and 3.07 ± 0.03 Å in **[Fe$_6$S$_6$]t$_4$$^{4-}$** and **[Fe$_6S_6$]t$_{40}$$^{4-}$**, respectively). Nevertheless, the $Fe_p-C(O)$ distance in **[Fe$_6$S$_6$]t$_{40}$$^{4-}$** is significantly longer than that observed in the X-ray structure of the enzyme.

As observed for **[Fe$_6$S$_6$]b$_1$$^{4-}$**, spin densities, atomic charges, and DOS analysis show that in the reduction **[Fe$_6$S$_6$]t$_1$$^{3-}$** + $e^- \rightarrow$ **[Fe$_6$S$_6$]t$_1$$^{4-}$** the added electron is partially delocalized over the entire H-cluster. However, and differently from **[Fe$_6$S$_6$]b$_1$$^{4-}$**, the excess of spin density on the $[2Fe]_H$ unit is localized on the Fe_p atom. The added electron becomes progressively more localized on the $[2Fe]_H$ cluster in **[Fe$_6$S$_6$]t$_4$$^{4-}$** and **[Fe$_6S_6$]t$_{40}$$^{5-}$**.

The exchange coupling constant J_{cube} calculated for **[Fe$_6$S$_6$]t^{4-}** is 328 ± 9, 382 ± 7, and 391 ± 6 cm^{-1} for ϵ = 1, 4, and 40, respectively. Similarly to $[Fe_6S_6]b_1^{4-}$, the energy gap between frontier orbitals in **[Fe$_6$S$_6$]t$_1$$^{4-}$** is very small (about 0.2 eV), and slightly increases in **[Fe$_6$S$_6$]t$_4$$^{4-}$** and **[Fe$_6S_6$]t$_{40}$$^{4-}$**. Therefore, also for this isomer, specific modifications of the environment might be expected to invert the order of stability of the frontier orbitals.

The stability of **[Fe$_6$S$_6$]t^{4-}** and **[Fe$_6$S$_6$]b^{4-}** is very similar (within 1.5 kcal mol^{-1}; Table S2 in the Supporting Information), indicating that the two isomers can coexist. In this respect, the influence of the Fe_4S_4 cluster is similar to that given by the coordination of a CH_3SH group to the Fe_p atom (**[Fe$_2$S$_2$(H)]b^{2-}** and **[Fe$_2$S$_2$(H)]b^{2-}**; Tables S33 and S36 in the Supporting Information). Instead, optimization of **[Fe$_2$S$_2$]t^{3-}** always converges to the μ-CO isomer.

[(SCH$_3$)$_4$(Fe$_4$S$_4$) (μ-pdt)(Fe$_2$)(CO)$_3$(CN)$_2$]$^{5-}$. Monoelectron reduction of $[Fe_6S_6]^{4-}$ leads to the $[(CH_3S)_4Fe_4S_4)(\mu$-pdt$)(Fe_2)(CO)_3(CN)_2]^{5-}$ complex (**[Fe$_6$S$_6$]$^{5-}$**), a model of the super-reduced state (H_{sred}) of the enzyme observed by Albracht et al. for reduction beyond −487 mV.[7c] This species could correspond either to a [Fe(I), Fe(I)]−[3Fe(II), Fe(III)] or to a [Fe(I), Fe(0)]−[2Fe(II), 2Fe(III)] redox state.

All attempts to obtain a DFT optimized structure of **[Fe$_6$S$_6$]b$_1$$^{5-}$** failed due to dissociation of the Fe_4S_4 cluster. In addition, optimization of the **[Fe$_6$S$_6$]t$_{40}$$^{5-}$** complex converged to the μ-CO isomer **[Fe$_6$S$_6$]b$_{40}$$^{5-}$**. Thus, μ-CO and all-terminal CO isomers are both stable species only when ϵ = 4.

In **[Fe$_6$S$_6$]b$_4$$^{5-}$** and **[Fe$_6S_6$]b$_{40}$$^{5-}$**, the geometry of the $[2Fe]_H$ cluster is nearly identical to that calculated for **[Fe$_6$S$_6$]b$_4$$^{4-}$** and **[Fe$_6S_6$]b$_{40}$$^{4-}$** (Table S1 in the Supporting Information). However, the geometrical parameters of the Fe_4S_4 cluster are similar to those computed for the $[(SCH_3)_4Fe_4S_4]^{-3}$ complex (**[Fe$_4$S$_4$]$^{3-}$**) in the same environment (Tables S1 and S40 in the Supporting Information).

Analysis of spin populations shows that the unpaired electron is always fully localized on the Fe_4S_4 cluster (Table 1), which, therefore, should be in the fully reduced +1 state. The net charge of the $\{Fe_4S_4(CH_3S)_4\}$ moiety (about −2.6) further confirms the assignment of the formal [Fe(I), Fe(I)]−[3Fe(II), Fe(III)] redox state for **[Fe$_6$S$_6$]b^{5-}**.

The B' value calculated for **[Fe$_6$S$_6$]b$_4$$^{5-}$** is 536 cm^{-1} and slightly increases to 556 cm^{-1} in **[Fe$_6$S$_6$]b$_{40}$$^{5-}$**. These values are about 70 cm^{-1} lower than those calculated for $[Fe_4S_4]^{3-}$ (Table 2). The exchange coupling constant J_{cube} changes from 360 to 376 cm^{-1} going from **[Fe$_6$S$_6$]b$_4$$^{5-}$** to **[Fe$_6S_6$]b$_{40}$$^{5-}$**, and it is slightly lower than in **[Fe$_4$S$_4$]$^{3-}$** (Supporting Information).

The highest occupied, as well as the lowest unoccupied, α and β orbitals in **[Fe$_6$S$_6$]b$_4$$^{5-}$** are all localized on the Fe_4S_4 cluster (Figure 5). Therefore, **[Fe$_6$S$_6$]b^{5-}** does not have frontier orbitals localized on the $[2Fe]_H$ unit that can be involved in the catalytic mechanism.[46]

In the $[(CH_3S)_4(Fe_4S_4)(\mu$-pdt$)(Fe_2)(CO)_3(CN)_2]^{5-}$ isomer **[Fe$_6$S$_6$]t$_1$$^{5-}$**, the Fe_d atom has a trigonal bipyramidal geometry and the $Fe_d(CO)_2(CN)$ group is partially rotated, with a CO ligand oriented toward the Fe_p atom ($C(O)-Fe_p$ distance = 3.23 Å). The Fe_d-Fe_p distance and the $Fe_1-S_b-Fe_p$ angle are as large as 2.72 Å and 156 ± 3°, respectively. Environment effects have a strong influence on the structure of **[Fe$_6$S$_6$]t^{5-}**, as expected due to its large negative charge. In fact, when moving from **[Fe$_6$S$_6$]t$_1$$^{5-}$** to **[Fe$_6S_6$]t$_4$$^{5-}$** the geometry of the $[2Fe]_H$ cluster converges to that calculated for $[Fe_6S_6]t_4^{4-}$, with the only exception of rotation of the $Fe_d(CO)_2(CN)$ group, which brings the CO ligand at a distance of about 2.8 Å from the Fe_p atom. In **[Fe$_6$S$_6$]t$_{40}$$^{5-}$**, the effect of the environment is even more drastic, and the only stable form corresponds to a structure characterized by a μ-CO group.

The analysis of spin densities, atomic charges (Table 2), and DOS profiles (not shown) shows that the electronic structure of **[Fe$_6$S$_6$]t^{5-}** is very similar to that described for **[Fe$_6$S$_6$]b^{5-}**. Finally, the **[Fe$_6$S$_6$]b$_4$$^{5-}$** and **[Fe$_6S_6$]t$_4$$^{5-}$** isomers are almost isoenergetic (Table S2 in the Supporting Information).

[(SCH$_3$)$_4$(Fe$_4$S$_4$)(μ-pdt)(Fe$_2$)(H)(CO)$_3$(CN)$_2$]$^{3-/4-}$. According to the most plausible mechanism for H_2 formation,[5,12a] protonation of the H-cluster should take place on the Fe_d atom in the H_{red} form of the enzyme. Protonation should be coupled to monoelectron reduction of the H-cluster. These observations prompted us to investigate, as potential intermediates in the catalytic cycle, the diamagnetic $[(SCH_3)_4(Fe_4S_4)(\mu$-pdt$)(Fe_2)(H)(CO)_3(CN)_2]^{3-}$ (from hereafter referred to as **H[Fe$_6$S$_6$]b^{3-}**), and the paramagnetic $[(SCH_3)_4(Fe_4S_4)(\mu$-pdt$)(Fe_2)(H)(CO)_3(CN)_2]^{4-}$ (**H[Fe$_6$S$_6$]b^{4-}**) complexes, which are obtained according to the reactions **[Fe$_6$S$_6$]b^{4-}** + $H^+ \rightarrow$ **H[Fe$_6$S$_6$]b^{3-}**, and **H[Fe$_6$S$_6$]b^{3-}** + $e^- \rightarrow$ **H[Fe$_6$S$_6$]b^{4-}**, respectively. We also investigated the

(46) For $[Fe_6S_6]b_4^{5-}$, the DOS profile of the $[2Fe]_H$ cluster (part e of Figure S1, panel III) is similar to that of $[Fe_6S_6]b_4^{4-}$ but shifted to lower energy with respect to the Fermi level. As expected by the change in the redox state, the DOS profile of the Fe_4S_4 cluster differs significantly from that of $[Fe_6S_6]b^{4-}$ or $[Fe_6S_6]b^{3-}$ (part e of Figure S1, panel II).

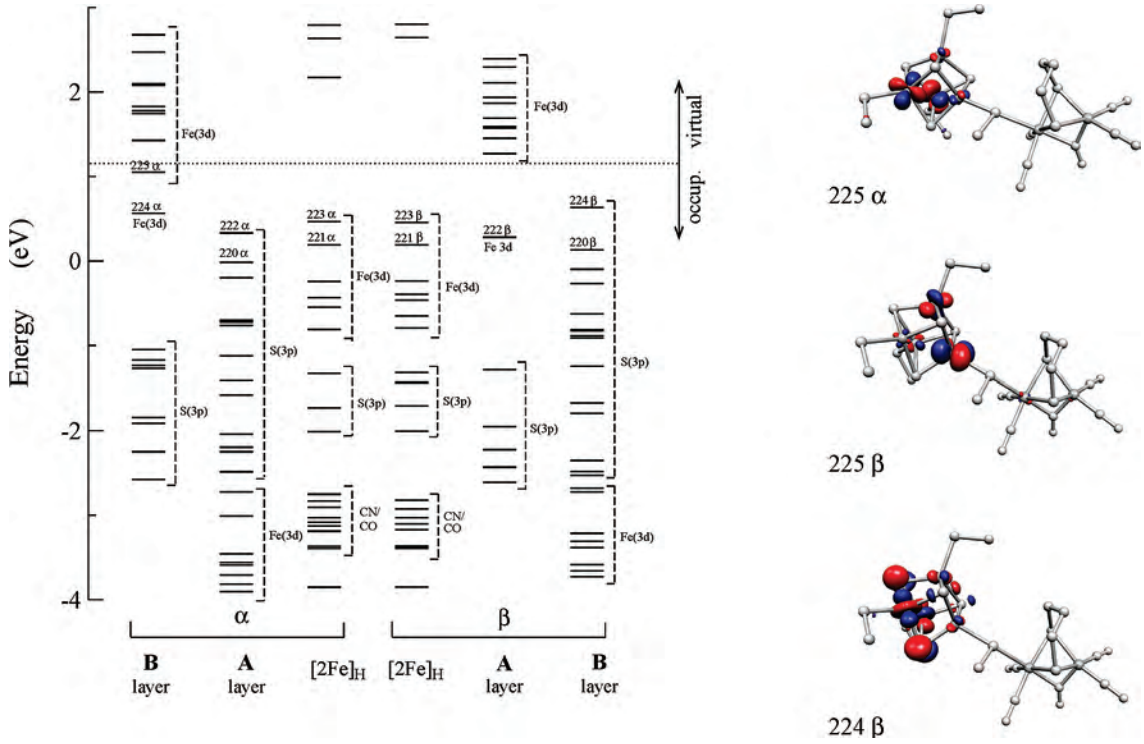

Figure 5. Detailed orbital diagram of the BS_1 state of $[Fe_6S_6]b_4^{5-}$. The labels and the description of the diagram have been given in the caption of Figure 2. On the right, the isodensity surfaces of some relevant molecular orbitals are also shown. In particular, **225α** is the highest-occupied α orbital (Fe−Fe bonding minority spin−orbital) localized on the **B** layer, which is filled in the reduction from $[Fe_6S_6]b_4^{4-}$ to $[Fe_6S_6]b_4^{5-}$. Orbitals **225*β*** and **224*β*** are the lowest-unoccupied and highest-occupied β orbitals localized on the **A** and **B** layers, respectively.

corresponding μ-H species $H[Fe_6S_6]t^{3-}$ and $\mathbf{H[Fe_6S_6]t^{4-}}$ to evaluate the effect of the Fe_4S_4 cluster on the relative stabilities of the two isomers.

Protonation of the Fe_d atom in $\mathbf{[Fe_6S_6]b^{4-}}$ affects the geometry of the $[2Fe]_H$ cluster. In particular, in $\mathbf{H[Fe_6S_6]b^{3-}}$ the Fe_p-Fe_d distance shortens by 0.09 Å, and the $Fe_d-C(O)$ distance lengthens by 0.06 Å, relative to $\mathbf{[Fe_6S_6]b^{4-}}$ (Supporting Information). The geometrical parameters of the cubane cluster are almost identical to those calculated for $\mathbf{[Fe_4S_4]^{2-}}$, suggesting a fully oxidized +2 state for the Fe_4S_4 core. The environment does not affect significantly the structure of the $[2Fe]_H$ cluster, with the only exception of the $Fe_1-S_b-Fe_p$ angle, which decreases by about 11° going from $\mathbf{H[Fe_6S_6]b_1^{3-}}$ to $\mathbf{H[Fe_6S_6]b_{40}^{3-}}$.

The influence of the Fe_4S_4 cluster on the structure of the protonated $[2Fe]_H$ cluster is evaluated by comparing the geometry of $\mathbf{H[Fe_6S_6]b^{3-}}$ with that of $[(SCH_3)(\mu\text{-pdt})(\mu\text{-CO})(Fe_2)(H)(CO)_2(CN)_2]^{2-}$ (hereafter referred to as $\mathbf{H[Fe_2S_2]b^{2-}}$) and $[(SHCH_3)(\mu\text{-pdt})(\mu\text{-CO})(Fe_2)(H)(CO)_2(CN)_2]^{1-}$ (hereafter referred to as $\mathbf{H[Fe_2S_2(H)]b^{1-}}$). In $\mathbf{H[Fe_2S_2]b^{2-}}$ and $\mathbf{H[Fe_2S_2(H)]b^{1-}}$, the presence of a proton coordinated to Fe_d affects the complex geometry similarly to what is observed for $\mathbf{H[Fe_6S_6]b^{3-}}$; the Fe_p-Fe_d distance significantly shortens, and the bridging CO slightly moves toward a semibridging position (Table S30 in the Supporting Information).

The analysis of spin and charge populations confirms the observations made in light of geometrical parameters. In fact, the net spin (∼0) and charge (−1.50) of the $\{Fe_4S_4(CH_3S)_4\}$ moiety in $\mathbf{H[Fe_6S_6]b^{3-}}$ are fully compatible with the formal +2 redox state of the Fe_4S_4 core.

The orbital correlation diagram and DOS profiles of $H[Fe_6S_6]b_4^{3-}$ differ from those computed for $\mathbf{[Fe_6S_6]b_4^{4-}}$ (Figure 6 and Figure S1 in the Supporting Information). In fact, protonation of the Fe_d atom gives rise to an electronic configuration in which the frontier orbitals are localized on the Fe_4S_4 cluster. In addition, the DOS profile of the Fe_4S_4 cluster in $\mathbf{H[Fe_6S_6]b_4^{3-}}$ is nearly identical to that of $\mathbf{[Fe_6S_6]b_4^{3-}}$, further confirming that the cubane in the two complexes has the same electronic structure.

Protonation of the $\mathbf{[Fe_6S_6]t^{4-}}$ complex gives an adduct in which the hydride ion is asymmetrically bridged between the two iron atoms. The Fe_p-Fe_d distance is 2.62 Å, about 0.1 Å longer than in $\mathbf{H[Fe_6S_6]b_1^{3-}}$. The electronic structure of $\mathbf{H[Fe_6S_6]t^{3-}}$ is very similar to that described for $\mathbf{H[Fe_6S_6]b^{3-}}$, and therefore it will be not discussed.

The energy difference between $\mathbf{H[Fe_6S_6]b^{3-}}$ and $\mathbf{H[Fe_6S_6]t^{3-}}$ is 11 kcal mol^{-1} in favor of $H[Fe_6S_6]t^{3-}$ and slightly decreases to about 7 kcal mol^{-1} when $\epsilon = 40$. This energy difference is in between that calculated for the corresponding bimetallic complexes in which the Fe_4S_4 cluster is replaced by CH_3S^- ($\mathbf{H[Fe_2S_2]b^{2-}}$, $\Delta E \approx -7$ kcal mol^{-1}) and CH_3SH groups ($\mathbf{H[Fe_2S_2(H)]b^{1-}}$; $\Delta E \approx -13$ kcal mol^{-1}).

Monoelectron reduction of $\mathbf{H[Fe_6S_6]b^{3-}}$ leads to the paramagnetic $\mathbf{H[Fe_6S_6]b^{4-}}$ complex, which might also be an intermediate species in the catalytic cycle. In $\mathbf{H[Fe_6S_6]b_1^{4-}}$, the Fe_p-Fe_d distance lengthens by about 0.07 Å, relative to $H[Fe_6S_6]b_1^{3-}$, and the bridging CO moves toward the Fe_p atom, assuming a more symmetrical arrangement (Table S3 in the Supporting Information). The average

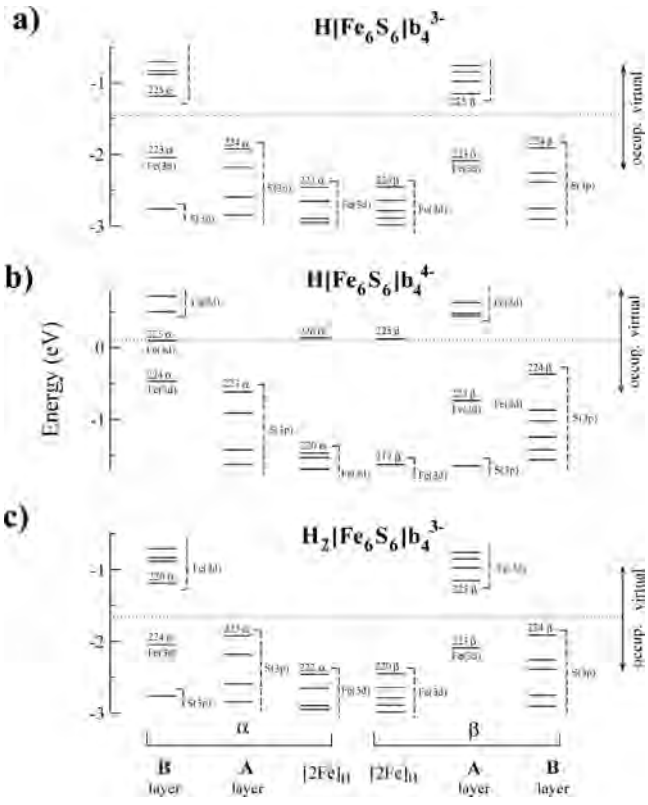

Figure 6. Orbital diagrams of (a) $\mathbf{H[Fe_6S_6]b_4^{3-}}$, (b) $\mathbf{H[Fe_6S_6]b_4^{4-}}$, and (c) $\mathbf{H[Fe_6S_6]b_4^{3-}}$, complexes with a few relevant occupied and unoccupied molecular orbitals (for comments, see the text).

Fe−Fe distance in the cubane cluster is 2.71 Å, a value in between those calculated for $\mathbf{[Fe_4S_4]_1^{2-}}$ and $\mathbf{[Fe_4S_4]_1^{3-}}$. Interestingly, when $\mathbf{H[Fe_6S_6]b_1^{4-}}$ is optimized in a polarizable continuum medium with $\epsilon = 4$ and 40, the geometrical parameters of the $[2Fe]_H$ cluster closely resemble those of $\mathbf{H[Fe_6S_6]b^{3-}}$, whereas the Fe−Fe distances in the cubane become more similar to those of $\mathbf{[Fe_4S_4]^{3-}}$.

The analysis of spin populations (Table 3) reveals that in $\mathbf{H[Fe_6S_6]b_1^{4-}}$ both the Fe_4S_4 and $[2Fe]_H$ clusters are characterized by a significant net spin density. In addition, the charge of the $\{Fe_4S_4(CH_3S)_4\}$ moiety is −2.17, a value compatible with a redox state of the Fe_4S_4 core intermediate between +1 and +2. These observations clearly suggest that the electron added in the reduction $\mathbf{H[Fe_6S_6]b_1^{3-}} + e^- \rightarrow \mathbf{H[Fe_6S_6]b_1^{4-}}$ is delocalized over the entire H-cluster. The spin on the $[2Fe]_H$ cluster is removed in $\mathbf{H[Fe_6S_6]b_4^{4-}}$ and $\mathbf{H[Fe_6S_6]b_{40}^{4-}}$, and the unpaired electron becomes fully localized on the Fe_4S_4 cluster, which therefore can be formally described as a [Fe(II)Fe(II)]−[3Fe(II), Fe(III)] subunit.

The orbital correlation diagram and DOS profiles (Figure 6 and Figure S1 in the Supporting Information) show that the highest occupied orbitals are localized on the Fe_4S_4 cluster. Instead, the lowest unoccupied orbitals are localized on the $[2Fe]_H$ cluster and very close in energy to the highest occupied ones. Therefore, similarly to the $\mathbf{[Fe_6S_6]b^{4-}}$ complex, a specific modification of the environment of $\mathbf{H[Fe_6S_6]b^{4-}}$ (such as protonation of a base in the neighborhood of the H-cluster)[47] can promote electron transfer from the Fe_4S_4 to the $[2Fe]_H$ cluster. In this contest, it is also important to note that the lowest unoccupied α and β orbitals (**226α** and ***225β*** in part b of Figure 6) are characterized by a significant contribution from the hydride ion. Thus, inversion of the frontier orbitals should give rise to an electronic configuration in which the hydride ion can act as a base for proton binding and subsequent H_2 evolution.

The structure of the $[2Fe]_H$ cluster in $\mathbf{H[Fe_6S_6]t^{4-}}$ is very similar to that discussed for $\mathbf{H[Fe_6S_6]t^{3-}}$, and the Fe_4S_4 structure is compatible with a redox state intermediate between +1 and +2. Analysis of spin and charge populations leads to the same conclusions obtained for $\mathbf{H[Fe_6S_6]b_4^{4-}}$; a significant spin delocalization is present in $\mathbf{H[Fe_6S_6]t_1^{4-}}$, which is progressively removed upon increasing the dielectric constant (Table 3). The electronic structure of $\mathbf{H[Fe_6S_6]t^{4-}}$ is also very similar to that discussed for $\mathbf{H[Fe_6S_6]b^{4-}}$, and therefore it will not be discussed.

The μ-H isomer $\mathbf{H[Fe_6S_6]t^{4-}}$ is more stable than $\mathbf{H[Fe_6S_6]b^{4-}}$ by about 8 kcal mol^{-1}, a value independent from the dielectric constant of the environment (Table S2 in the Supporting Information).

$[(SCH_3)_4(Fe_4S_4)(\mu\text{-pdt})(Fe_2)(H_2)(CO)_3(CN)_2]^{3-}$. Protonation of the hydride group in $\mathbf{H[Fe_6S_6]b^{4-}}$ leads to the paramagnetic $[(SCH_3)_4(Fe_4S_4)(\mu\text{-pdt})(Fe_2)(H_2)(CO)_3(CN)_2]^{3-}$ complex (hereafter referred to as $H_2[Fe_6S_6]b^{3-}$), which is characterized by a H_2 molecule coordinated to the Fe_d atom. In $\mathbf{H_2[Fe_6S_6]b_1^{3-}}$ the Fe_p-Fe_d distance is 2.67 Å, a value more than 0.07 and 0.1 Å larger than that calculated for $\mathbf{H[Fe_6S_6]b_1^{4-}}$ and $\mathbf{[Fe_6S_6]b_1^{3-}}$, respectively. The bridging CO moves toward the Fe_p atom ($Fe_p-C(O) = 1.89$ Å and $Fe_d-C(O) = 2.04$ Å). The H−H bond in H_2 is slightly activated (0.823 Å).

The geometrical parameters of the $[2Fe]_H$ cluster in $\mathbf{H_2[Fe_6S_6]b^{3-}}$, which are in between those calculated for the dinuclear $\mathbf{H_2[Fe_2S_2]b^{2-}}$ and $\mathbf{H_2[Fe_2S_2]b^{1-}}$ model complexes (Tables S3 and S32 in the Supporting Information), are not strongly affected by an increase of the dielectric constant, with the exception of the $Fe_1-S_b-Fe_p$ angle and S_b-Fe_p distance, which considerably decrease when going from $\mathbf{H_2[Fe_6S_6]b_1^{3-}}$ to $\mathbf{H_2[Fe_6S_6]b_{40}^{3-}}$ (Table S3 in the Supporting Information). The geometrical parameters of the Fe_4S_4 cluster in $\mathbf{H_2[Fe_6S_6]b^{3-}}$ are compatible with a fully oxidized +2 redox state.

The analysis of atomic spin densities shows that the unpaired electron is fully localized on the $[2Fe]_H$ cluster. However, differently from the $\mathbf{[Fe_6S_6]b^{3-}}$ complex, the unpaired electron is delocalized between the Fe_p (0.49) and Fe_d (0.43) atoms. The spin densities, as well as the net charge of the cubane cluster (≈ −1.6), are consistent with the +2 redox state.[48]

H_2 binding leading to $\mathbf{H_2[Fe_6S_6]b_1^{3-}}$ is endothermic by about 5.5 kcal mol^{-1}, a value which decreases to 2.9 kcal mol^{-1} when considering $\mathbf{H_2[Fe_6S_6]b_{40}^{3-}}$ (Table S2 in the Supporting Information). Again, these energy values are in between those calculated for the corresponding bimetallic complexes $\mathbf{H_2[Fe_2S_2]b^{2-}}$ and $\mathbf{H_2[Fe_2S_2]b^{1-}}$.

(47) Indeed, if the pdt chelating ligand is replaced with protonated dtma, the stability order of the frontier orbitals is actually inverted, and an electron transfer takes place from the Fe_4S_4 to the $[2Fe]_H$ cluster (manuscript in preparation).

Table 3. Atomic Spin Densities of the Iron atoms of the $\mathbf{H[Fe_6S_6]^{3-}}$, $\mathbf{H[Fe_6S_6]^{4-}}$, and $\mathbf{H_2[Fe_6S_6]^{3-}}$ Models Computed at the BP86/def-TZVP Level of Theory[a]

		$\mathbf{H_2[Fe_6S_6]b^{3-}}$	$\mathbf{H_2[Fe_6S_6]t^{3-}}$	$\mathbf{H[Fe_6S_6]b^{3-}}$	$\mathbf{H[Fe_6S_6]t^{3-}}$	$\mathbf{H[Fe_6S_6]b^{4-}}$	$\mathbf{H[Fe_6S_6]t^{4-}}$
				Atomic Spin Densities			
$Fe_{1,2}$	$\epsilon = 1$	3.11*,3.09	3.12*,3.10	3.14*,3.09	3.10*,3.09	3.27*,3.19	3.24*,3.19
	$\epsilon = 4$	3.07*,3.07	3.06*,3.07	3.05*,3.07	3.05*,3.07	3.16*,3.18	3.18*,3.19
	$\epsilon = 40$	3.06*,3.06	3.05*,3.07	3.03*,3.07	3.04*,3.06	3.14*,3.19	3.15*,3.20
$Fe_{3,4}$	$\epsilon = 1$	−3.10,−3.09	−3.12,−3.09	−3.12,−3.10	−3.13,−3.09	−2.80,−3.11	−2.97,−3.09
	$\epsilon = 4$	−3.08,−3.06	−3.07,−3.05	−3.08,−3.06	−3.10,−3.06	−2.97,−2.87	−2.85,−2.92
	$\epsilon = 40$	−3.06,−3.05	−3.06,−305	−3.06,−3.05	−3.08,−3.04	−2.83,−2.84	−2.85,−2.84
Fe_p	$\epsilon = 1$	0.47	0.50	0.04	0.05	0.35	0.25
	$\epsilon = 4$	0.47	0.42	0.04	0.05	0.19	0.10
	$\epsilon = 40$	0.47	0.42	0.04	0.05	0.05	0.04
Fe_d	$\epsilon = 1$	0.46	0.38	0.01	0.01	0.10	0.15
	$\epsilon = 4$	0.45	0.44	0.01	0.01	0.07	0.05
	$\epsilon = 40$	0.43	0.43	0.01	0.01	0.01	0.01
				Atomic Charges			
$Fe_{1,2}$	$\epsilon = 1$	0.22*,0.16	0.21*,0.18	0.23*,0.17	0.21*,0.17	0.25*,0.23	0.25*,0.22
	$\epsilon = 4$	0.24*,0.14	0.25*,0.14	0.23*,0.14	0.21*,0.15	0.27*,0.19	0.26*,0.20
	$\epsilon = 40$	0.25*,0.13	0.27,*0.13	0.26*,0.13	0.21*,0.14	0.30*,0.18	0.30*,0.18
$Fe_{3,4}$	$\epsilon = 1$	0.17,0.17	0.18,0.17	0.16,0.18	0.18,0.16	0.21,0.21	0.22,0.21
	$\epsilon = 4$	0.15,0.15	0.14,0.14	0.15,0.14	0.16,0.15	0.17,0.18	0.19,0.18
	$\epsilon = 40$	0.14,0.13	0.13,0.14	0.13,0.13	0.15,0.13	0.15,0.15	0.16,0.16
Fe_p	$\epsilon = 1$	−0.49	−0.49	−0.50	−0.50	−0.44	−0.45
	$\epsilon = 4$	−0.48	−0.51	−0.52	−0.49	−0.49	−0.46
	$\epsilon = 40$	−0.48	−0.51	−0.53	−0.48	−0.51	−0.47
Fe_d	$\epsilon = 1$	−0.56	−0.61	−0.67	−0.68	−0.62	−0.62
	ϵ=4	−0.54	−0.59	−0.65	−0.67	−0.61	−0.65
	$\epsilon = 40$	−0.55	−0.59	−0.65	−0.67	−0.63	−0.66
q_b^{Fe4S4}	$\epsilon = 1$	−1.62	−1.61	−1.51	−1.56	−2.17	−2.20
	$\epsilon = 4$	−1.58	−1.56	−1.47	−1.54	−2.22	−2.36
	$\epsilon = 40$	−1.57	−1.56	−1.46	−1.53	−2.36	−2.45

[a] $Fe_{1,2}$ and $Fe_{2,3}$ refer to the iron atoms of the two layers coupled antiferromagnetically in the $[Fe_4S_4]$ cluster; Fe_p and Fe_d refer to the proximal and distal iron atoms of the $[2Fe]_H$ cluster, respectively. [b] Net charge of the $\{Fe_4S_4(CH_3S)_4\}$ moiety in the H-cluster.

The isomer $\mathbf{H_2[Fe_6S_6]t^{3-}}$ is formed upon binding of H_2 to the Fe_p atom of $\mathbf{[Fe_6S_6]t^{3-}}$. In this complex, the Fe_p-Fe_d distance is as long as 2.85 Å, and it is not affected by the value of ϵ. H_2 is highly activated, as indicated by the large H−H distance (0.98 Å). The electronic structure of $\mathbf{H_2[Fe_6S_6]t^{3-}}$ is similar to that described for $\mathbf{H_2[Fe_6S_6]b^{3-}}$. In fact, geometrical parameters (Supporting Information), atomic spin densities, and atomic charges (Table 3) are consistent with the cubane cluster in the fully oxidized state, and the $[2Fe]_H$ cluster in the Fe(I)Fe(II) state. In addition, as observed for $\mathbf{H_2[Fe_6S_6]b^{3-}}$, the unpaired electron is delocalized between the Fe_p and Fe_d atoms.

It is interesting to note that H_2 binding to $\mathbf{[Fe_6S_6]t^{3-}}$, to give $\mathbf{H_2[Fe_6S_6]t^{3-}}$, is more endothermic than the corresponding reaction, leading to $H_2[Fe_6S_6]b^{3-}$. $\mathbf{H_2[Fe_6S_6]t^{3-}}$ is also less stable than $\mathbf{H_2[Fe_6S_6]b^{3-}}$ (Table S2 in the Supporting Information).

Discussion

The theoretical study described in this work reports on a detailed analysis of the electronic structure of the entire H-cluster in different redox and protonation states. The most relevant findings can be summarized as follows:

1. The large negative charge of the H-cluster leads, in a vacuum, to structures of the $[2Fe]_H$ subcluster significantly different from those observed experimentally in the protein. In particular, for all of the species investigated the $Fe_1-S_b-Fe_p$ angle is larger than that in the X-ray structures. Inclusion of averaged environment effects leads to much better agreement with experimental data, indicating that the protein environment is able to solvate the large negative charge of the H-cluster. Remarkably, analysis of the protein structure shows that there are only two charged residues (Lys237 and Glu240 in *D. desulfuricans* X-ray structure), involved in a salt-bridge interaction, in the proximity of the H-cluster.

2. The exchange interaction between the Fe_4S_4 and the $[2Fe]_H$ clusters and the value of the $Fe_1-S_b-Fe_p$ angle are strongly correlated, suggesting that the value of the $Fe_1-S_b-Fe_p$ angle can be considered an internal report of the electronic structure of the H-cluster. Such a correlation is particularly evident for the H_{ox} models $\mathbf{[Fe_6S_6]b^{3-}}$ and $\mathbf{[Fe_6S_6]t^{3-}}$, where the exchange coupling constant J_H increases significantly upon decreasing the $Fe_1-S_b-Fe_p$ angle.

3. The comparison of Fe_6S_6 and Fe_2S_3 DFT models shows that the presence of the Fe_4S_4 moiety does not strongly affect the geometry of the $[2Fe]_H$ cluster.

4. Both $\mathbf{[Fe_6S_6]b^{4-}}$ and $\mathbf{[Fe_6S_6]t^{4-}}$ complexes do not reproduce accurately the peculiar semibridging position of a CO ligand observed in the X-ray structure of the H_{red} form in the enzyme. The same holds true for the corresponding bimetallic model complexes. However, it must be noted that the potential energy surface along the reaction coordinate

(48) The DOS profile of the Fe_4S_4 cluster is very similar to that calculated for $[Fe_6S_6]b^{3-}$, further indicating that in $H_2[Fe_6S_6]b^{3-}$ the electronic configuration of the Fe_4S_4 cluster is not affected by H_2 binding. On the other hand, some differences are observed for the DOS of the $[2Fe]_H$ cluster. In particular, the orbital containing the unpaired electron rises in energy and becomes the highest occupied orbital.

Scheme 1. Reactivity of the H-Cluster as Predicted by DFT Calculations[a]

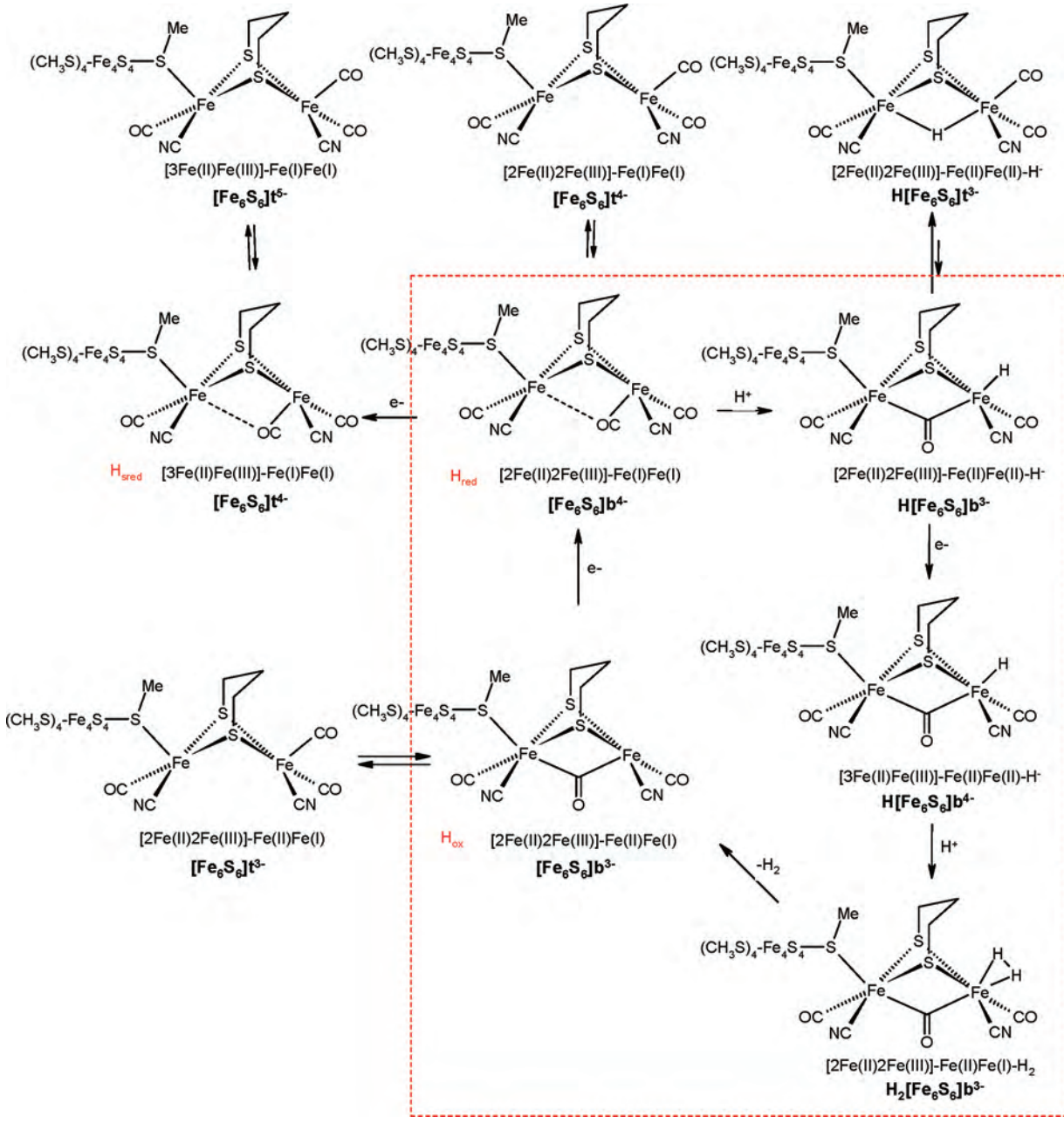

[a] Species relevant for the catalytic mechanism of H_2 formation are in the red dotted box.

corresponding to μ-CO movement is quite flat, suggesting that subtle effects not reproduced by our calculations can strongly affect the position of the bridging CO ligand.

5. As for the relative stability of μ-CO versus all-terminal CO isomers, both **[Fe$_6$S$_6$]b^{3-}** and **[Fe$_6$S$_6$]t^{3-}** (H_{ox} models) and [Fe$_6$S$_6$]b^{4-} and [Fe$_6$S$_6$]t^{4-} (H_{red} models) isomers are almost isoenergetic, similar to what observed for the corresponding Fe_2S_3 complexes. Therefore, the Fe_4S_4 cluster alone cannot be invoked to explain the stabilization of the μ-CO forms (observed in the enzyme) relative to all-terminal CO isomers.

6. Protonation of the H_{red} form of the H-cluster can occur at the Fe_d atom, in trans to μ-CO, giving a terminal hydride, or at the Fe_p-Fe_d bond, giving a μ-H hydride. The μ-H species are always more stable than the terminal hydride isomers. In particular, even though the computed reaction energy for the **H[Fe$_6$S$_6$]b^{3-}** → **H[Fe$_6$S$_6$]t^{3-}** isomerization becomes less favorable upon increasing the dielectric constant of the environment, H[Fe$_6$S$_6$]t^{3-} remains significantly more stable than H[Fe$_6$S$_6$]b^{3-}. Analogous considerations hold true for the **H[Fe$_6$S$_6$]b^{4-}** and **H[Fe$_6$S$_6$]t^{4-}** isomers. In light of these results, it can be concluded that specific interactions of the H-cluster with the environment, not considered in our calculations, are necessary to reverse the stability order of μ-H and terminal hydrides or that terminal protonation at the Fe_d atom is a kinetically controlled event.

7. The analysis of molecular orbitals and DOS profiles has provided information on the electronic structure of the

H-cluster, as well as on the electronic communication between the two subclusters. In all of the complexes investigated, the orbital configuration of the Fe_4S_4 cluster can be assigned to the so-called inverted scheme, in which Fe(3d) orbitals lie lower in energy than S(3p) orbitals. However, the contribution of other orbitals is not negligible, as expected by the covalent character of the Fe−S bond, indicating that the picture of the electronic structure drawn only on the basis of ligand field arguments is rather inadequate in this case. The electronic structure of the $[2Fe]_H$ cluster is always characterized by a normal scheme, in which Fe(3d) orbitals are higher in energy than S(3p) orbitals.

8. The DOS profiles projected on the Fe_4S_4 cluster can be used as a signature of its redox state and reveal that in **[Fe$_6$S$_6$]b^{3-}** and **[Fe$_6$S$_6$]b^{5-}** the Fe_4S_4 moiety is in the fully oxidized ($[Fe_4S_4]^{+2}$) and fully reduced ($[Fe_4S_4]^{+1}$) redox state, respectively. Moreover, the projected DOS profiles of the **H$_2$[Fe$_6$S$_6$]b^{3-}** and **H[Fe$_6$S$_6$]b^{3-}** complexes clearly indicate that the Fe_4S_4 moiety remains in the fully oxidized state (Scheme 1). The same holds true for **[Fe$_6$S$_6$]b^{4-}** when $\epsilon \geq 4$, whereas when $\epsilon = 1$ the DOS of **[Fe$_6$S$_6$]b^{4-}** are characterized by a profile in between those of $[Fe_6S_6]b^{3-}$ and **[Fe$_6$S$_6$]b^{5-}**, corresponding to partial reduction of the Fe_4S_4 core from the +2 to the +1 redox state. Finally, the DOS profile of **H[Fe$_6$S$_6$]b^{4-}** is fairly similar to that of **[Fe$_6$S$_6$]b^{5-}**, indicating an almost complete reduction of the Fe_4S_4 core to the +1 redox state (Scheme 1).

9. The atomic charges of the Fe_p and Fe_d atoms are nearly symmetrical in the μ-CO complexes, whereas they are more asymmetric in complexes featuring all terminal COs. Most importantly, atomic charges of the Fe_p and Fe_d atoms are not markedly affected by the formal oxidation state of the H-cluster (Table 1). In particular, the charge of Fe_d remains almost unchanged when going from **[Fe$_6$S$_6$]b^{3-}** to **[Fe$_6$S$_6$]b^{5-}**. These observations can account for the difficulties in assigning the redox state of the iron atoms using Mössbauer spectroscopy.[7a,b]

Whereas the structural features of the $[2Fe]_H$ cluster in the entire H-cluster do not differ significantly from those computed for the corresponding bimetallic model complexes, results obtained for the different redox and protonation states show that the H-cluster has peculiar characteristics when reactivity properties are considered:

10. A description of a plausible catalytic mechanism for [FeFe] hydrogenases (Scheme 1) can be started from the model of the H_{red} form of the enzyme (**[Fe$_6$S$_6$]b^{4-}**), which is characterized by highest-occupied and lowest-unoccupied molecular orbitals very close in energy and localized on the $[2Fe]_H$ and Fe_4S_4 clusters, respectively. In light of this latter observation, protonation of **[Fe$_6$S$_6$]b^{4-}** should lead to **H[Fe$_6$S$_6$]b^{3-}**, where the Fe_4S_4 cluster is in the fully oxidized state and the highest-occupied and lowest-unoccupied orbitals are localized on the Fe_4S_4 cluster. As a consequence, the $[2Fe]_H$ cluster in **H[Fe$_6$S$_6$]b^{3-}** is not expected to be able to bind another proton because the first occupied orbital localized on the $[2Fe]_H$ subcluster is about 1 eV lower in energy than the highest occupied one. Addition of one electron to **H[Fe$_6$S$_6$]b^{3-}** leads to the reduction of the Fe_4S_4 cluster (Scheme 1). In **H[Fe$_6$S$_6$]b^{4-}**, the occupied orbitals localized on the $[2Fe]_H$ subcluster are still very low in energy and therefore should not be expected to play a role in catalysis. However, the lowest unoccupied α orbital is localized on the $[2Fe]_H$ subcluster and is characterized by a significant contribution from the hydride ion. The energy difference between this orbital and the highest occupied α and β orbitals is very small and subtle modifications of the dielectric constant of the environment can reverse the order of stability of the frontier orbitals,[47] providing an electron transfer path from the Fe_4S_4 to the $[2Fe]_H$ cluster. The inversion of the orbitals stability would provide an occupied orbital localized on the $[2Fe]_H$ cluster suitable to act as a base, in a reaction channel leading to protonation of **H[Fe$_6$S$_6$]b^{4-}** and subsequent H_2 evolution (Scheme 1). Indeed, protonation of **H[Fe$_6$S$_6$]b^{4-}** leads to **H$_2$[Fe$_6$S$_6$]b^{3-}**, in which molecular hydrogen is still bound to the Fe_d atom. In **H$_2$[Fe$_6$S$_6$]b^{3-}**, the Fe_4S_4 cluster is in the fully oxidized state. Dissociation of H_2 from $H_2[Fe_6S_6]b^{3-}$ is exothermic by a few kcal mol^{-1} and leads to $[Fe_6S_6]b^{3-}$. It is interesting to note that the orbital configuration of **[Fe$_6$S$_6$]b^{3-}** (which corresponds to the H_{ox} form of the enzyme) is fully compatible with reversible binding of H_2 at the free coordination site because there is a low-lying unoccupied orbital that can act as an acceptor. Finally, monoelectron reduction of **[Fe$_6$S$_6$]b^{3-}** to give **[Fe$_6$S$_6$]b^{4-}** closes the catalytic cycle.

11. Monoelectron reduction of $[Fe_6S_6]b^{4-}$ leads to the paramagnetic $[Fe_6S_6]b^{5-}$ species, which should correspond to the super-reduced form (H_{sred}) observed by Albracht et al.[7c] In this complex, the Fe_4S_4 cluster is in the reduced +1 state, whereas the $[2Fe]_H$ cluster remains in the Fe(I)Fe(I) state (Scheme 1). This means that the Fe(I)Fe(0) state of $[2Fe]_H$ cluster is inaccessible in the enzyme even at very low potential, a result that further highlights the differences between the entire H-cluster and most bimetallic complexes synthesized so far, which can promote H_2 evolution through a mechanism involving the Fe(I)Fe(0) state.

12. Finally, we have observed that binding of ligands such as H_2 (this work), H^+, CO, or H_2O (unpublished results) at the vacant coordination site of **[Fe$_6$S$_6$]b^{3-}** gives rise to delocalization of the unpaired electron between the iron atoms of the $[2Fe]_H$ cluster, independently from the ϵ value. However, in **[Fe$_6$S$_6$]b^{3-}** the unpaired electron is completely localized on the Fe_d atom, in good agreement with Mössbauer data obtained on the H_{ox} form of the enzyme.[7a,b] Therefore, it can be concluded that the H_{ox} form of the enzyme should correspond to a species characterized by a vacant coordination site at the Fe_d atom.

These observations are expected not only to contribute to a better understanding of the enzyme chemistry but also to be useful for the design of synthetic complexes resembling the structural and functional properties of the enzyme cofactor. In particular, our results are consistent with a scenario in which subtle differences in the H-cluster environment may tune the electronic structure of the cofactor and therefore affect the activity/directionality of the enzyme, as recently underlined by Lubitz and co-workers.[49]

Acknowledgment. The authors thank Federico Totti and Alessandro Bencini for fruitful discussions.

Supporting Information Available: Energies, relevant geometrical parameters, and DOS profiles of all of the species considered in this study. This material is available free of charge via the Internet at http://pubs.acs.org.

IC8006298

(49) Silakov, A.; Reijerse, E. J.; Albracht, S. P. J.; Hatchikian, E. C.; Lubitz, W. *J. Am. Chem. Soc.* **2007**, *129*, 11447.